Atmos. Meas. Tech. Discuss., 8, 4917–4971, 2015
www.atmos-meas-tech-discuss.net/8/4917/2015/
doi:10.5194/amtd-8-4917-2015

Atmospheric Measurement Techniques Discussions

Explorative study on GOME-2 total column ozone retrievals and the validation with ground-based and balloon measurements

A. Wassmann, T. Borsdorff, J. M. J. aan de Brugh, O. P. Hasekamp, I. Aben, and J. Landgraf

Netherlands Institute for Space Research SRON, Sorbonnelaan 2, 3584 CA Utrecht, the Netherlands

Received: 23 March 2015 – Accepted: 24 April 2015 – Published: 13 May 2015

Correspondence to: A. Wassmann (a.wassmann@sron.nl)

Published by Copernicus Publications on behalf of the European Geosciences Union.

Abstract

In this work we present an extensive sensitivity study of retrieved total ozone columns from clear sky Global Ozone Monitoring Experiment 2 (GOME-2) measurements between 325 and 335 nm which are corrected for instrument degradation. Employing an algorithm based on the scaling of a reference ozone profile with the extension to analytically calculate total column averaging kernels, allows us to investigate the impact of the choice of the reference profile on the retrieved total ozone column, since it represents a regularization of the retrieval. It introduces an error to the retrieved column with respect to the true column typically in the order of 1 % depending on the reference scaling profile. However, a proper interpretation of the retrieved column using the total column averaging kernel avoids this error, which is demonstrated by a validation of GOME-2 total ozone columns with collocated ozonesonde and ground-based total ozone column measurements. Globally, we report a bias of 0.1 % and a SD of 2.5 % for 647 collocations with ground-based and ozonesonde measurements at different geolocations in the period of 2007 to 2010. Futhermore, an extended validation solely based on ground-based observations and a strict cloud filtering shows that the use of pseudo spherical scalar radiative transfer is fully sufficient for the purpose of this retrieval. Polarization of light by atmospheric scattering affects the retrieval accuracy only marginally and thus can be ignored. Finally, we study the effect of instrument degradation on the retrieved total ozone columns for the first four years of GOME-2 observations and discuss the efficiency of the proposed radiometric correction.

1 Introduction

Ozone is an important constituent of Earth's atmosphere and monitoring its atmospheric abundance is essential to improve our understanding on tropospheric chemistry, air quality and climate change. For this purpose, satellite measurements in the ultraviolet (UV) part of the solar spectrum between 310 and 340 nm form a valuable

AMTD
8, 4917–4971, 2015

tool to measure the vertically integrated amount of ozone with global coverage. The Global Ozone Monitoring Experiment 2 (GOME-2) aboard the three European Sun-synchronous, polar-orbiting MetOp satellites, with two currently in operation and the third one due for launch in 2017, measures earth radiance and solar irradiance spectra in the UV, visible, and near infrared spectral range from 240 to 790 nm with a spectral resolution of 0.24–0.53 nm and a spectral sampling of 0.11–0.22 nm. It continues a long heritage starting with the Solar Backscatter UltraViolet instruments (SBUV and SBUV/2) (Bhartia et al., 1996) and the Total Ozone Mapping Spectrometer (TOMS) (Bhartia and Wellemeyer, 2004) on Nimbus 7 launched in 1978, followed in Europe by GOME (Burrows et al., 1999) on ERS-2 in 1995, the Scanning Imaging Absoption Spectrometer for Atmospheric CHartographY (SCIAMACHY) (Bovensman et al., 1999) on Envisat in 2002, and the Ozone Monitoring Instrument (OMI) (Levelt, 2006) on Aura in 2004.

To retrieve total ozone columns from these instruments, different algorithms have been developed. Most of the algorithms employ the Differential Optical Absorption Spectroscopy (DOAS) technique (e.g. Coldewey-Egbers et al., 2005; Weber et al., 2005; Eskes et al., 2005; Van Roozendael et al., 2006; Veefkind et al., 2006; Loyola et al., 2011), which is benificial with respect to its computational cost. Alternatively, Lerot et al. (2010, 2014) have proposed a non-linear least squares fitting algorithm, which adjusts a scaling to a reference ozone profile to fit UV radiance measurements. Borsdorff et al. (2014) proposed an important extension of this approach by describing an efficient manner to analytically calculate the total column averaging kernel for each individual retrieval. This quantity describes the sensitivity of the retrieved column with respect to changes in the vertical ozone distribution and it is an essential component for a proper interpretation of this type of satellite observations.

For GOME-2 the operational O3MSAF/EUMETSAT ozone column product is based on the DOAS method (Valks et al., 2013) and is extensively validated with ground-based measurements. Antón et al. (2009) performed a validation over the Iberian Peninsula using Brewer spectrometer measurements and found a bias of −3.05 %, while

AMTD
8, 4917–4971, 2015

Loyola et al. (2011) report a global mean bias and SD of -0.28 ± 0.7 % with respect to Dobson spectrometer measurments and -1.22 ± 0.67 % with respect to Brewer spectrometer measurements. A comparison with the total ozone columns from GOME, SCIAMACHY, and OMI showed biases of −0.8, −0.37, −1.28 %, respectively, ensuring a consistent dataset (Koukouli et al., 2012). Furthermore, degradation of satellite instruments in the UV is often observed (e.g. GOME and SCIAMACHY). Several methods have been published to correct measured reflectances with modeled reflectances (e.g. van der A et al., 2002; Krijger et al., 2005; van Soest et al., 2005) or by comparing measured reflectances to those at the beginning of the misson after removing both, solar zenith angle and seasonal dependencies (Liu et al., 2007). Cai et al. (2012) provide an extensive analysis of both the spectral and the cross-track degradation of GOME-2 measurements with time compared with model simulations. This so-called "soft" calibration is also implemented in the retrieval of SO_2 from GOME-2 measurements (Nowlan et al., 2011).

In this study, we investigate the sensitivity of retrieved total ozone columns to a set of key parameters, such as the choice of the scaling ozone profile, instrument degradation, cloudiness, topography, the approximation of Earth's sphericity, and the choice of the radiative transfer solver. Therefore, we model earth radiances, calculate the reflectance, and use a least squares profile scaling approach of a reference profile to retrieve total ozone columns from GOME-2 measurements. Moreover, following Borsdorff et al. (2014), we analytically calculate the total column averaging kernel for each retrieval and apply it for the validation of the data product. This approach allows us to investigate the impact of the ozone profile used for scaling on the contribution of the null space of the retrieval. The null space comprises that part of the state vector that cannot be retrieved from the measurements. We investigate the impact of the degradation of GOME-2 measurements on the retrieval product. The degradation is solely derived from global cloud free measurements referenced to 2007, which is also the first year of the mission. For this purpose, we assume that the mean reflectance over a certain area for the same observation geometry and time of the year does not change

AMTD
8, 4917–4971, 2015

for a cloud free atmosphere. Finally, we analyse the retrieval sensitivity with respect to cloudiness, topography, the approximation of Earth's sphericity, and the choice of the radiative transfer solver and validate our retrieval algorithm with ground-based Brewer, Dobson and Système d' Analyse par Observation Zénithale (SAOZ) spectrometer data and collocated ozonesonde measurements.

The paper is structured as follows: in Sect. 2 we briefly describe the forward model and the inversion scheme. Section 3 describes the radiometric correction of the GOME-2 measurements to mitigate the instrument degradation. In Sect. 4 we present and discuss the validation of our GOME-2 retrieval algorithm with a number of ground stations regarding the choice of the reference ozone profile (Sect. 4.1), followed by an analysis of the influence of a set of key parameters on the validation such as cloudiness, topography, the approximation of Earth's sphericity, the choice of the radiative transfer solver, and scan mirror degradation in Sect. 4.2. Finally, in Sect. 5 we conclude this paper.

2 Algorithm description and retrieval setup

2.1 Forward model

To retrieve total ozone columns from GOME-2 measurements, a forward model $\mathbf{F}_{\text{earth}}$ is needed in order to simulate GOME-2 earth radiance measurements $\boldsymbol{y}_{\text{earth}}$ as

$$\boldsymbol{y}_{\text{earth}} = \mathbf{F}_{\text{earth}}(\boldsymbol{x}, \boldsymbol{b}) + \boldsymbol{e}_{\text{earth}} . \quad (1)$$

$\mathbf{F}_{\text{earth}}$ is a function of the state vector $\boldsymbol{x}$ to be retrieved and the model parameter vector $\boldsymbol{b}$, which contains additional parameters that influence the spectrum but are not altered by the inversion. The error vector $\boldsymbol{e}_{\text{earth}}$ combines both, errors in the measurement and forward model errors.

The forward model $\mathbf{F}_{\text{earth}}$ requires a solar spectrum $\boldsymbol{S}_0$ sampled on an internal, fine spectral grid. To infer $\boldsymbol{S}_0$ from the daily GOME-2 solar irradiance measurements $\boldsymbol{y}_{\text{sun}}$,

AMTD
8, 4917–4971, 2015

we set up a forward model equation analogous to Eq. (1) but for the solar measurement, where we assume that the solar measurement $\boldsymbol{y}_{\text{sun}}$ can be simulated by spectral convolution of the solar spectrum $\boldsymbol{S}_0$ with the instrument spectral response function. This yields the forward model equation for the solar spectrum

$$\boldsymbol{y}_{\text{sun}} = \mathbf{K}_{\text{ISRF}}\boldsymbol{S}_0 + \boldsymbol{e}_{\text{sun}}\,. \tag{2}$$

The matrix $\mathbf{K}_{\text{ISRF}}$ represents the convolution of the solar spectrum with the instrument spectral response function and $\boldsymbol{e}_{\text{sun}}$ is the corresponding error vector. In Eq. (2), the length of the observation vector $\boldsymbol{y}_{\text{sun}}$ is smaller than the length of $\boldsymbol{S}_0$ and so its inversion has no unique solution. Van Deelen et al. (2007) showed that the least squares minimum length solution $\hat{\boldsymbol{S}}_0$, which minimizes the length of the solution vector $\hat{\boldsymbol{S}}_0$ as a side constraint, is of sufficient accuracy to simulate earth radiance measurements of the GOME mission. Following this approach, we calculate the earth radiance measurements by

$$\mathbf{F}_{\text{earth}}(\hat{\boldsymbol{S}}_0) = \mathbf{K}_{\text{ISRF}}(\boldsymbol{r}\cdot\hat{\boldsymbol{S}}_0) \tag{3}$$

where we explicitly show the dependence of $\mathbf{F}_{\text{earth}}$ on the solar spectrum and omit any other dependence. Furthermore, $\boldsymbol{r}$ is the spectral reflectance of Earth's atmosphere. Equation (3) assumes the same instrument spectral response function for solar irradiance and earth radiance measurements, and so the noise contribution on the inferred solar spectrum $\hat{\boldsymbol{S}}_0$ is attenuated by the convolution in Eq. (3).

The transfer of light through Earth's atmosphere is described by the reflectance $\boldsymbol{r}$ as part of the convolution

$$(\boldsymbol{r}\cdot\hat{\boldsymbol{S}}_0)(\lambda) = \int \mathrm{d}\widetilde{\lambda}\, r(\lambda,\widetilde{\lambda})\,\hat{\boldsymbol{S}}_0(\widetilde{\lambda})\,. \tag{4}$$

It includes the description of inelastic Raman scattering and elastic Rayleigh scattering of solar light, where the integral kernel $r(\lambda,\widetilde{\lambda})$ represents the reflection of sunlight at the

AMTD
8, 4917–4971, 2015

incoming wavelength $\widetilde{\lambda}$ to the outgoing wavelength λ. Numerical calculations of r are very time-consuming (e.g. Landgraf et al., 2004; van Deelen et al., 2005) and thus require an approximation to keep the numerical effort of the algorithm reasonable. Based on the concept of pre-calculated Ring spectra (e.g. Hoogen et al., 1999; Hasekamp and Landgraf, 2001; Lerot et al., 2014), we approximate Eq. (4) by

$$\mathbf{F}_{\text{earth}}(\hat{\boldsymbol{S}}_0) \approx \boldsymbol{r}_{\text{Ray}} \cdot \hat{\boldsymbol{S}}_0 \left(1 + a \frac{\boldsymbol{r}^{\text{LUT}}_{\text{Ram}} \cdot \hat{\boldsymbol{S}}_0}{\boldsymbol{r}^{\text{LUT}}_{\text{Ray}} \cdot \hat{\boldsymbol{S}}_0} \right) \tag{5}$$

where $\boldsymbol{r}_{\text{Ray}}$ is the monochromatic earth reflectance due to atmospheric Rayleigh scattering. It is calculated online employing the LINTRAN radiative transfer model (Landgraf et al., 2001; Walter et al., 2004; Hasekamp et al., 2005; Schepers et al., 2014). For all simulations, we use ozone cross sections by Brion et al. (1993) as well as scattering cross sections and phase matrices for Rayleigh scattering described by Bucholtz (1995). LINTRAN comprises a scalar and vector radiative transfer solver in plane parallel geometry and its pseudo-spherical extension. In this study, we employ the scalar solver with the pseudo-spherical approximation if not mentioned differently. Additionally, $\boldsymbol{r}^{\text{LUT}}_{\text{Ray}}$ and $\boldsymbol{r}^{\text{LUT}}_{\text{Ram}}$ are pre-calculated reflectances stored in a lookup table, which includes Rayleigh scattering and inelastic Raman scattering, respectively. The lookup table is calculated with the model by Landgraf et al. (2004) for the US standard atmosphere, a nadir viewing geometry, a Lambertian surface albedo $A_{\text{s}} = 0.1$ and it includes the dependence on the total ozone column and solar zenith angle. Factor a in Eq. (5) is a free model parameter to adjust the effect of Raman scattering in the retrieval.

The use of the reflectance lookup tables $\boldsymbol{r}^{\text{LUT}}_{\text{Ram}}$ and $\boldsymbol{r}^{\text{LUT}}_{\text{Ray}}$ in Eq. (5) instead of pre-calculated Ring spectra bears the advantage that the simulation is based on one solar spectrum, which eases the spectral calibration of the forward model. Assuming the molecular spectroscopy of ozone as spectral reference, the forward model can be spectrally adjusted by shifting the solar spectrum in Eq. (5), $\hat{\boldsymbol{S}}_0(\lambda) \rightarrow \hat{\boldsymbol{S}}_0(\lambda + \Delta\lambda_{\text{S}})$, and by a corresponding spectral adjustment of the instrument spectral response function

AMTD
8, 4917–4971, 2015

$s(\lambda, \widetilde{\lambda}) \rightarrow s(\lambda + \Delta\lambda_{\mathrm{ISRF}}, \widetilde{\lambda})$. Both, the spectral calibration $\Delta\lambda_{\mathrm{S}}$ and $\Delta\lambda_{\mathrm{ISRF}}$ are elements of the state vector and are determined by the inversion module, which is discussed in the next section.

2.2 Inversion module

For the inversion, we need to linearize the forward model around an initial guess of the state vector $\boldsymbol{x}_0$,

$$\boldsymbol{y} = \mathbf{K}\boldsymbol{x} + \boldsymbol{e}_{\mathrm{earth}}, \tag{6}$$

where $\mathbf{K} = \partial\mathbf{F}/\partial\boldsymbol{x}$ is the Jacobian matrix and $\boldsymbol{y} = \boldsymbol{y}_{\mathrm{earth}} - \mathbf{F}(\boldsymbol{x}_0, \boldsymbol{b}) + \mathbf{K}\boldsymbol{x}_0$. Both, the simulated radiance and the Jacobian are standard outputs of the LINTRAN radiative transfer model. To retrieve the total ozone column, we follow the profile scaling approach used by Lerot et al. (2010). The state vector consists of the total ozone column c, the surface albedo A_{s} and its spectrally linear dependence δA_{s}, the amplitude a in Eq. (5), a spectral shift of the solar spectrum $\Delta\lambda_{\mathrm{S}}$, and a spectral shift of the instrument spectral response function $\Delta\lambda_{\mathrm{ISRF}}$ in Eq. (3). Here, the column density c is defined by vertical profile integration,

$$c = \mathbf{C}^{\mathrm{T}}\boldsymbol{\rho}, \tag{7}$$

where $\mathbf{C} = (1, \ldots, 1)$ represents the corresponding geometric integration assuming an ozone profile ρ given in partial column densities per model layer.

We apply Eq. (6) to invert Eq. (1) in an iterative way with respect to the state vector $\boldsymbol{x}$ using Gauss–Newton iteration, for which the minimization problem

$$\hat{\boldsymbol{x}} = \min_{x} \left\{ \left\| \mathbf{S}_{\mathbf{e}}^{-1/2}(\mathbf{K}\boldsymbol{x} - \boldsymbol{y}) \right\|_2^2 \right\} \tag{8}$$

is solved in each iteration step. Here $\|\cdot\|_2$ represents the L_2 norm and $\mathbf{S}_{\mathbf{e}}$ is the measurement error covariance. For this purpose, the Jacobian with respect to a scaling

AMTD
8, 4917–4971, 2015

of a reference profile is calculated from corresponding derivatives with respect to an altitude resolved ozone profile $\boldsymbol{\rho}$,

$$\mathbf{K}_i^{\text{col}} = \frac{\partial F_i}{\partial c} = \sum_j K_{ij}^{\text{prof}} \frac{\rho_j^{\text{ref}}}{c^{\text{ref}}}. \tag{9}$$

Here, $K_{ij}^{\text{prof}} = \partial F_i / \partial \rho_j$ describes the profile Jacobian, ρ_j represents the ozone sub-column of the profile in layer j, and ρ^{ref} is the reference profile used for the scaling approach. From Eq. (9) it is clear that the profile scaling approach relies on an altitude resolved profile Jacobian. A direct analytical calculation of the derivative $\partial F_j / \partial c$ is not possible due to scattering and the temperature dependence of the ozone absorption. $\mathbf{K}^{\text{col}}$ together with the derivatives of the measurement with respect to the other elements of the state vector defines the column of the least squares Jacobian $\mathbf{K}_{\text{lsq}}$ and the solution of Eq. (8) is given by

$$\hat{\boldsymbol{x}} = \mathbf{G}_{\text{lsq}} \boldsymbol{y} \tag{10}$$

with the gain matrix

$$\mathbf{G}_{\text{lsq}} = \left(\mathbf{K}_{\text{lsq}}^{\text{T}} \mathbf{S}_{\mathbf{e}}^{-1} \mathbf{K}_{\text{lsq}} \right)^{-1} \mathbf{K}_{\text{lsq}}^{\text{T}} \mathbf{S}_{\mathbf{e}}^{-1}. \tag{11}$$

The least squares scaling approach can be interpreted as a regularized retrieval of the vertical ozone distribution (Borsdorff et al., 2014). Hence, the retrieved column $\hat{c}$ represents an estimate of an altitude weighted integration of the true ozone profile, namely

$$\hat{c} = \mathbf{A}^{\text{col}} \rho_{\text{true}} + e_{\text{col}} \tag{12}$$

where $\mathbf{A}^{\text{col}}$ is the total column averaging kernel, ρ_{true} is the true ozone profile and e_{col} is the error on the retrieved column due to the measurement error $\boldsymbol{e}_{\boldsymbol{y}}$. This means that

AMTD
8, 4917–4971, 2015

generally the retrieved column $\hat{c}$ should be interpreted as an estimate of the effective column

$$c_{\text{eff}} = \mathbf{A}^{\text{col}} \rho_{\text{true}} \,. \tag{13}$$

The part of the true column that cannot be inferred from the measurement, namely

$$e_{\text{n}} = (\mathbf{C} - \mathbf{A}^{\text{col}}) \rho_{\text{true}} \,, \tag{14}$$

belongs to the effective null space of the inversion and is also known as smoothing error of the retrieval (Rodgers, 2000). Borsdorff et al. (2014) discussed the meaning of this error term. They showed that the null space contribution of the reference profile ρ_{ref} is always zero, $\mathbf{A}^{\text{col}} \rho_{\text{ref}} = \mathbf{C}\,\boldsymbol{\rho}_{\text{ref}}$. Consequently,when the correct relative profile is used for the scaling approach, the retrieved column can be interpreted as an estimate of the true column. In other words, the null space contribution e_{n} is the error due to the choice of the reference profile.

To infer the total column averaging kernel in our algorithm, we follow the approach by Borsdorff et al. (2014). Interpreting the profile scaling approach as a particular case of a regularized profile retrieval using Tikhonov regularization of the first order with an infinitely strong regularization, Borsdorff et al. (2014) showed that the gain matrix reduces to a gain vector $\boldsymbol{g}^{\text{col}}$ representing the fitted ozone column, which in turn we can extract from the gain matrix of the least-squares fit $\mathbf{G}_{\text{lsq}}$ and calculate the total column averaging kernel

$$\mathbf{A}^{\text{col}} = \left(\frac{\mathrm{d}c}{\mathrm{d}\rho_i} \right) = \boldsymbol{g}^{\text{col}} \mathbf{K}^{\text{prof}} \,. \tag{15}$$

For the proof of Eq. (15), the reader is referred to Borsdorff et al. (2014).

Based on these findings, one may follow two different philosophies to derive a GOME-2 ozone column product: the first approach aims to provide an estimate of the true column. Starting with accurate a priori knowledge on the relative vertical distribution of ozone, the retrieved column is an estimate of the true column and the total

AMTD
8, 4917–4971, 2015

column averaging kernel is not needed for the data interpretation. Here, the data product depends critically on the quality of the a priori knowledge of the ozone profile. For validation purposes, the retrieved column can then be directly compared to total ozone columns inferred from ground-based spectrometer measurements, which are recorded routinely as part of a global measurement network. This strategy is widely used in the literature, e.g. by Lerot et al. (2014). Alternatively, one may provide the effective ozone column together with the total column averaging kernel. In this case, Eq. (13) represents the basis for validation, and hence an estimate of the vertical ozone profile is needed. Ozonesonde measurements can be used for this purpose. However, due to fewer observation sites and less frequent measurements, a corresponding validation is limited in its temporospatial coverage. Obviously, the advantage of this approach is the minor dependence of the data product on the a priori knowledge of the vertical ozone distribution. Important applications, like the assimilation of the total ozone column in global and regional models, preferably deal with information purely coming from the measurements and thus try to minimize the effect of ozone knowledge originating from a priori data. For such applications, the effective column together with its total column averaging kernel forms a well suited data product.

Figure 1 shows the total column averaging kernels for retrievals from simulated measurements. Here, the measurements are simulated for an ozonesonde profile on 15 January 2009 over De Bilt, the Netherlands, representing the true ozone profile. Retrievals are performed for three different reference ozone profiles, the US standard ozone profile (NOAA, 1976), the corresponding profile extracted from the climatology by Fortuin and Kelder (1998), which provides monthly averaged climatological ozone profiles in 10° latitude bands, and the true ozone profile. All are depicted in the right panel of Fig. 1 as dashed line, dotted line, and solid line, respectively. Although the US standard and the climatological reference profile of Fortuin and Kelder (1998) peak at different altitudes with different magnitudes, one can see in the left panel that the general shape of the total column averaging kernel is largely similar. The null space contribution of the sonde profile clearly differs for the given model atmosphere and is

AMTD
8, 4917–4971, 2015

e_n = 0.12 % for the US standard ozone profile and e_n = −0.95 % for the climatological profile, respectively. It vanishes when the ozonesonde profile itself is used as reference profile as expected. Depending on the reference profiles, we thus can expect errors in the order of 1 % when we interpret the retrieved column as an estimate of the true column. This error source can be avoided when we interpret the retrieved column as an effective column and subsequently apply the total column averaging kernel concept for validation. In Sect. 4.1 we demonstrate this aspect by applying both concepts to GOME-2 measurements.

Finally for the retrieval, we use temperature and pressure profiles from the European Centre for Medium-Range Weather Forecasts (ECMWF) ERA interim data (Berrisford et al., 2009) as auxiliary input and assume a clear sky atmosphere by filtering for cloudiness. This cloud filter is based on FRESCO cloud parameters (Wang et al., 2008), which are part of the disseminated GOME-2 level 1B product, and is discussed in detail in Sect. 4.2.

3 Instrument degradation

To validate the presented algorithm, we apply it to spectra recorded by GOME-2/MetOp-A between January 2007 and July 2011, disseminated by EUMETSAT. Due to the choice of the retrieval window between 325–335 nm, we only use data from channel 2B with the advantage of the small 80 × 40 km ground pixels. Because of the optical degradation of the GOME-2 scan mirror, the reflectance measurements are subject to a spectral radiometric error. To mitigate this error, two major approaches are reported in the literature, one based on the predictability of the measurement using radiative transfer simulations and a priori knowledge about the atmospheric state and the other based on actual measurements, assuming that the averaged radiometric signal over certain regions is constant for the same period of the year, i.e. surface albedo and observation geometry. For example, Cai et al. (2012) calculate the degradation as relative difference between measured data and modeled data in the wavelength region between 270 and

AMTD
8, 4917–4971, 2015

350 nm for the tropical belt (25° S–5° N), where ozone varies only little, for the period between February 2007 and December 2009 in 15 day intervals. For GOME, Liu et al. (2007) presented a different approach comparing measured reflectances with respect to those of a reference date. Assuming a constant mean reflectance value, they considered the mean reflectance measured between 60° N and 60° S as a function of time for the first and 15th day of each month. Subsequently, the mean reflectance is referenced to the value determined for 1 July 1995. To remove solar zenith angle dependency and other seasonality, two third-order polynomials in time are fitted to the data. There are several advantages of using observations only over a comparison with simulated measurements. First, no collocations of the radiative transfer input parameters with the measurements are needed and second, more importantly, uncertainties in ozone profiles, temperature profiles, and cloud data which lead to forward model errors are avoided. In that way only the effect of the instrument degradation and of atmospheric variations remain. However, averaging daily data over a large enough region reduces the impact of the latter.

In this paper, we follow a similar approach to Liu et al. (2007), monitoring degradation at three wavelengths in our total ozone fitting window, namely 325, 330, and 335 nm. For each of the wavelengths, we consider GOME-2 reflectances between 60° N–60° S with minor cloud contamination of cloud fraction $f_{cld} \leq 10\,\%$, which is calculated by the FRESCO cloud algorithm (Wang et al., 2008). We arrange the data in 5° latitude bins, 2° solar zenith angle bins, and 24 ground pixel bins representing the cross track scan. To define the degradation δI_{deg} for the period 2008–2011, the reflectance is referenced to the corresponding reflectance of the year 2007, which is also the first year of the mission, at the same day of the year for the same solar zenith angle bin, latitude bin and ground pixel bin. We observe a clear scan angle dependence, shown for 330 nm in Fig. 2. Here, ground pixel 2 represents the easternmost pixel, since pixel 1 is discarded due to poor statistics, and ground pixel 24 represents the westernmost pixel. One can clearly identify different rates at which the across track degradation takes place as indicated by the colour gradients. The westward pixels are subject to the most severe

AMTD
8, 4917–4971, 2015

degradation with about 9.5 % at the end of the period under investigation, while the eastward pixels are least affected (3–4 %), which is comparable to the findings of Tilstra et al. (2012). Based on these findings, we correct the relative radiometric degradation of GOME-2 radiances with respect to solar measurements assuming a multiplicative error contribution (R. Snel, personal communication, 2014, SRON, the Netherlands). Since the degradation showed only little spectral dependency across our fitting window, we consider it spectrally constant. From the data of Fig. 2, we derived a corresponding degradation correction for the period 2008–2011 per scan mirror position by linear regression. It is assumed that the GOME-2 data are not affected by the degradation in 2007 and hence are not corrected.

4 Validation

To validate the retrieval product, we employ Eq. (12), and hence, we rely on measurements of the vertical distribution of ozone, represented on the vertical grid of the model atmosphere (2 km thick model layers between 0 and 60 km). For this purpose, we use ozonesonde measurements which are extended with the climatology of Fortuin and Kelder (1998) above the sonde burst height and subsequently normalised to the total column of ozone of a collocated ground-based measurement. This approach accounts for both, the lack of data above the burst height and systematic errors resulting from differences in pre-flight preparation of the ozonesonde (Kerr et al., 1994; Beekmann et al., 1994, 1995; Smit et al., 1998; Fioletov et al., 2006). Both, ozonesonde measurements and ground-based data have to be recorded at the same day and spatially co-aligned within at least a radius of 0.5°. Additionally, we corrected the total column from ground-based measurements for the difference in surface elevation between the measurement site and the mean GOME-2 pixel elevation, which is derived from Shuttle Radar Topography Mission (SRTM) high-resolution digital topographic database (Farr et al., 2007) and the near-surface ozone mixing ratio approximated by the ozone reference profile.

AMTD
8, 4917–4971, 2015

Generally, much less ozonesonde measurements than ground-based measurements are available, which limits the number of validation measurements. However, a sufficient number of collocations has been found to evaluate the relevance of the total column averaging kernel. In total, we consider ozone measurements at 36 stations that are displayed in Fig. 3 and extracted the corresponding data from the WOUDC (see www.woudc.org) and SHADOZ (Thompson et al., 2007) networks. For some stations, more than one ground-based instrument was operational for the examined period, which allows us to intercompare different instrumentations. From Fig. 3, a good coverage of validation sites in the Northern Hemisphere is evident with an even higher density of stations in Europe, which is displayed in the zoom-in of the map. Details for each station are given in Table 1, showing the coordinates and the type of spectrometer.

The algorithm validation depends critically on the accuracy of the ground-based total column measurements of ozone. Fioletov et al. (2008) indicated less accuracy of zenith sky measurements and so we exclude these measurements in our study. Moreover, Basher (1982); Komhyr et al. (1989); Basher (1994); Kerr et al. (1997); Fioletov et al. (2005) reported that a precision of 1 % for well-calibrated Brewer and Dobson instruments can be reached. However, systematic differences of about ±0.6 % between both are introduced through different temperature dependencies of the absorption cross sections at the different wavelengths used by the instruments (Staehelin et al., 2003). For SAOZ instruments, Van Roozendael et al. (1998) carried out a validation with Dobson and Brewer instruments and found a bias of about 2 % between the two types of measurements. Thus differences between GOME-2 retrieval and ground-based measurements have to be considered in the view of this overall uncertainty of our validation measurements.

4.1 Validation of the effective ozone column product

To validate the GOME-2 effective ozone column product with collocated ozonesonde and ground-based measurements, we apply several quality criteria. First, we define

AMTD
8, 4917–4971, 2015

a cloud filter for GOME-2 measurements based on an effective cloudiness parameter

$$\eta_{\mathrm{cld}} = f_{\mathrm{cld}} \frac{z_{\mathrm{cld}}}{z_{\mathrm{ref}}}, \tag{16}$$

where f_{cld} is the factional cloud coverage of the observed scene, z_{cld} the cloud top height and z_{ref} a reference height. The effective cloudiness parameter yields largest values for high clouds and large cloud fraction and thus describes a shielding of the subjacent atmosphere. For the numerical implementation of the cloud screening, we employ the GOME-2 FRESCO cloud product (Wang et al., 2008) and assume a reference height $z_{\mathrm{ref}} = 10\,\mathrm{km}$. To filter on representation errors and errors due to scene heterogeneity, we consider three days of consecutive ground-based measurements, with the second day being spatio-temporally coregistrated with a GOME-2 measurement and the difference of that collocated ground-based measurement with the measurements of the preceding day and succeeding day (δt) has to be less than a threshold value. Measurements are assumed to be spatially co-aligned when the distance between the site of the ground-based measurements and the center of the GOME-2 pixel δr does not exceed a threshold. Moreover, only GOME-2 products are considered with $\chi^2 \leq \chi^2_{\mathrm{max}}$ of the spectral fitting. For the effective column validation, we choose strict quality filtering, based on

$$\delta t < 15\ \mathrm{DU} \tag{17}$$

$$\delta r < 300\ \mathrm{km} \tag{18}$$

$$\chi^2_{\mathrm{max}} = 2 \tag{19}$$

$$\eta_{\mathrm{cld}} < 0.1\,. \tag{20}$$

The dependence of the validation on the cloud filtering will be discussed in more detail in Sect. 4.2.

Figures 4 and 5 display two examples of the GOME-2 validation for ozone measurements at Naha, Japan, and Hohenpeissenberg, Germany. At both measurement

AMTD
8, 4917–4971, 2015

sites, direct sun measurements are performed with a Dobson and a Brewer instrument, respectively. In the following, we consider the two validation concepts discussed in Sect. 2.2: first, we compare the retrieved ozone column directly with the ground-based measurement (direct column comparison). Second, we compare the retrieved column with the effective column defined in Eq. (13) (effective column comparison).

The upper panel of Fig. 4 shows the time series of the retrieved total ozone column (filled circle) and the ground-based ozone column (open circle) for Naha, Japan. Here, we chose the US standard reference profile to be scaled by the retrieval. Overall, we see a good agreement between both total ozone columns with the same seasonal dependence. However, a closer look reveals that the direct comparison of the ozone columns is negatively biased by −2.6 % in its mean with a SD around the mean of 2.2 %. The mean bias is mainly caused by the choice of the US standard profile as reference profile. As discussed in Sect. 2.2, this effect is characterized by the total column averaging kernel and the corresponding null space error shown in the middle panel. The latter is estimated from the ozonesonde measurements scaled to the Dobson total ozone column and the total column averaging kernel of the individual retrievals (using Eq. 12). The null space error is on the order of 3 %, but varies between the different soundings because of the variability of the total column averaging kernel and the ozonesonde measurements with respect to the standard atmosphere. The lower panel of Fig. 4 shows the relative retrieval error for the direct and effective column comparison. It indicates the importance of the total column averaging kernel, where the mean retrieval bias is reduced to −0.2 % with a SD around the mean bias of 1.9 %. Similar results are obtained for Hohenpeissenberg, Germany (see Fig. 5). Here, the mean bias and the SD reduce from −1.8 and 2.3 % for the direct comparison to −0.7 and 2.2 %, respectively, for the effective column comparison.

Figures 4 and 5 are based on temporal and spatial collocations of ground-based Dobson and Brewer measurements, ozonesonde measurements and GOME-2 observations. Figure 6 shows the time series of GOME-2 and ground-based measurements for a set of stations with direct sun measurements and with more than 15 collocations

AMTD
8, 4917–4971, 2015

with GOME-2 retrievals. For each station, we consider the mean bias as a diagnostic tool, which is depicted in Fig. 7. We investigate the effect of three different choices for the reference profile in the inversion: (1) the ozone profile of the US standard atmosphere (2) climatological profiles of Fortuin and Kelder (1998) and (3) the collocated ozonesonde measurements.

Using the US standard reference profile, the mean retrieval bias varies from station to station between −0.8 and −3 % for the direct comparison. For all sites, the bias is reduced significantly for the effective column comparison with mean biases between 0.6 and −1.1 %. For climatology profiles, the performance of both approaches becomes similar with biases ranging from 0.7 to −1 %, however, the validation of GOME-2 retrievals improves significantly for Naha, Hong Kong Observatory, and Broadmeadows, when the null space contribution of the regularization is accounted for. Finally, using the ozonesonde profile as reference profile, provides identical results for direct and effective column comparison with biases of 1 to −0.9 %, because the null space contribution of the reference profile diminishes by definition (see discussion in Sect. 2.2). Moreover, the effective column comparison results in a very similar validation for the three choices of the reference profile. The SD of the retrieval error varies only little for the different approaches. This confirms that a proper treatment of the regularization of the profile scaling approach in the validation reduces the dependence of the validation on the particular shape of the reference profile.

For all 36 stations, we summarize the validation in Table 1 (dataset 1) by giving the number of collocations, the mean error, and the error SD. Here, collocated ozonesonde measurements were used as reference profile ρ_{ref}.

4.2 Column validation with ground-based measurements

Finally, we study the retrieval performance of the proposed algorithm as a function of a set of key parameters. For this purpose, the validation dataset of the previous section is too small and thus we discard the spatial coregistation of the GOME-2 observations with ozonesonde measurements at the cost of a proper estimate of the null space error.

AMTD
8, 4917–4971, 2015

To generate this second dataset, we relax the quality filter (Eq. 17) to $\delta t < 30$ DU and obtain a total of 6861 validation measurements that satisfy the cloudiness criterion in Eq. (20), which is about six times more than for the first validation dataset. For this dataset the reference ozone profiles are extracted from the climatology by Fortuin and Kelder (1998). The retrieval diagnostics using this dataset (dataset 2) are also given in Table 1 for all stations and Fig. 8 displays the corresponding retrieval biases for those stations that comprise at least 30 collocations. On global average, the difference between the observation modes of the ground-based spectrometer are minute with a mean bias of −0.1 % and an error SD of 2.7 %. Overall, we see similar biases for Dobson, Brewer and SOAZ instruments with largest biases for Scoresbysund (3.2 %), Macquarie Island (−2.3 %), and Marambio (3.3 %). In this analysis we do not account for the effective null space, and thus from the results of Fig. 7, we expect that the biases can be overestimated up to 1 %.

To investigate the retrieval performance as a function of key parameters, one has to consider the range of these parameters carefully by defining suitable subsets. The need to correct for topographic differences between validation site and satellite ground pixel is demonstrated exemplary for the elevated sites Izaña (∼ 2300 m a.s.l.) and Mauna Loa (∼ 3400 m a.s.l.). Here, we obtain retrieval biases of 0.2 and 1.1 % after correction as shown in Fig. 9, compared to −1.8 and −3.5 %, respectively, without elevation correction. For other stations the elevation correction is of minor importance due to smaller differences in elevation.

Next, we investigate the effect of cloudiness, as defined in Eq. (16), on our retrieval performance. Therefore, we consider the retrieval error for each station as a function of cloudiness and correct the data for an overall bias determined from nearly cloudfree scenes ($\eta_{\mathrm{cld}} < 0.1$). This correction varies between ±2 % depending on the validation site, which is reflected in the station-to-station bias variation in Fig. 8. Applying this correction, highlights the dependence of the retrieval bias on cloudiness η_{cld} as shown in Fig. 10. For $\eta_{\mathrm{cld}} \leq 0.1$ the relative dependence on cloudiness is weak but increases significantly for $\eta_{\mathrm{cld}} > 0.1$, showing already a retrieval error of about −1 % for $\eta_{\mathrm{cld}} = 0.15$

AMTD
8, 4917–4971, 2015

and further increases to $\Delta_{ret} = -3.2\,\%$ for $\eta_{cld} = 0.5$. This justifies the criterion for cloud filtering set in Eq. (20) in the previous section.

For satellite observations at large solar zenith angles, the treatment of Earth's sphericity as part of the radiative transfer simulation becomes an important aspect. We investigate the retrieval performance as a function of solar zenith angle for different approximations: (1) plane-parallel radiative transfer, (2) the air mass correction of Kasten and Young (1989) and (3) the pseudo-spherical approximation (Walter et al., 2004). Here, we select validation sites, where the GOME-2 measurements cover at least the solar zenith angles $50^\circ < \theta < 80^\circ$. To correct for overall biases, for each station the dataset is corrected for its mean error determined from solar zenith angles $\theta < 55^\circ$, which varies between −2 and 3 %. In this way, we consider the relative error at larger solar zenith angle. Figure 11 shows a clear improvement when using the pseudo-spherical approximation instead of the plane-parallel approximation with and without airmass correction. For $\theta > 70^\circ$, using the plane-parallel approximation underestimates the ozone column up to a mean error of 7.5 % at $\theta = 85^\circ$. Errors are reduced by more than a factor 2 using the air mass correction and about −0.5 % for pseudo-spherical approximation. This is in agreement with the sphericity effect studied for simulated measurements. Nevertheless, the relative error shows some suspicious features, e.g. the positive error of 2 % for the speudo-spherical simulations at $\theta = 77^\circ$. This may be caused by the combination of different measurement sites with different bias corrections. For a better comprehension of the solar zenith angle dependence, Fig. 12 shows the retrieval error as function of the solar zenith angle for three stations, Lerwick (Dobson), Uccle (Brewer) and Praha, which is equipped with a Dobson and a Brewer spectrometer. For each dataset, we determine a potential trend by linear regression. The SD of the data points with respect to the regression is used to characterize the overall quality of the regression. Although the validation sites are located at similar latitudes and hence GOME-2 covers a similar range of solar zenith angles, the datasets show different dependences. For both Dobson instruments at Lerwick and at Praha, we observe a clear positive trend with increasing solar zenith angle of 1.2

AMTD
8, 4917–4971, 2015

and 1 % per 10° solar zenith angle, respectively, whereas for the Brewer instruments at Uccle and at Praha such a trend is not present in the data, 0.2 and 0.1 %, respectively. Particularly for Praha, we conclude that the error trend is probably inflicted by the ground measurements and not by the GOME-2 data and one may suggest that the Praha Dobson spectrometer is more susceptible for solar zenith angle dependencies. Figure 13 summarizes the slope of the regression and the SD for all stations of Table 1 with sufficient data coverage. Significant slopes are observed for the stations Churchill (B-MKIV.032), Goose Bay, Praha (Dobson), Boulder, Tateno, and Ushuaha, which is confirmed by the small variation of the SD of the data points around the linear regression within the dataset. The trends in Fig. 13 indicate a significant error dependence on solar zenith angle for Dobson spectrometers. However, to confirm that a more thorough study is needed with stations comprising multiple instruments and sufficient data.

One may argue that the use of the scalar radiative transfer solver in our forward model, which does not include polarization properties of light, potentially causes the solar zenith angle error dependence. In the left panel of Fig. 14 the spectral error in the wavelength range between 303 and 336 nm is shown for different solar geometries and comprises a strong wavelength dependence for wavelengths smaller than 320 nm for almost all investigated scattering geometries. Here, the polarization of light is governed by singly scattered light, which for Rayleigh scattering has its highest degree of linear polarization for a scattering angle of $\Theta_{scat} = 90^{\circ}$. This polarization affects the intensity at higher scattering orders, and consequently causes an error on the simulated intensity if it is not accounted for. For the spectral window used in this study (325–335 nm), this error comprises mainly a radiometric offset but it also includes spectral features interfering with spectral absorption features of ozone, which is shown in the right panel for the same scattering geometry. To estimate the effect of the used scalar forward model on our retrieved ozone column product, we have generated synthetic measurements for all solar and measurement geometries of the Lerwick validation set, shown in Fig. 12, using a vector radiative transfer model. The geometries of Lerwick are used here exemplary, because the dataset comprises a good coverage for the geometries.

AMTD
8, 4917–4971, 2015

The errors in the total ozone columns caused by using a scalar radiative transfer model are shown in Fig. 15 as function of the scattering angle in single scattering geometry. In case we fit a spectrally constant effective albedo, as shown in the left panel, in order to account for the radiometric offset, the error on the total ozone column is substantial with a maximum of 4 % at a scattering angle $\Theta_{scat} = 90^{\circ}$, where the maximum error is expected to be. Here, the error pattern clearly follows the radiometric offset in Fig. 14. The retrieval error induced by using the scalar version of the forward model can be further reduced by fitting a linear spectrally dependent surface albedo, which is depicted in the right panel of Fig. 15. For almost all scattering angles the error diminishes and is below 0.7 % in all cases.

Although the effect of these forward model errors is small, it is interesting to see if the corresponding changes in the retrieved ozone columns improve the validation with ground measurements. For this purpose, we consider the retrieval error Δ_{ret} as function of the scattering angle Θ_{scat} using vector and scalar radiative transfer simulations. In Fig. 16, the linear regression through the data points shows a dependence on Θ_{scat} for the scalar radiative transfer model (middle panel), which reduces when vector radiative transfer is used (upper panel). In calculating the difference of Δ_{ret} between both radiative transfer models $\Delta_{sca} - \Delta_{vect}$, displayed in the bottom panel, the same structure, both in magnitude and position with respect to the scattering angles, as seen already in the right panel of Fig. 15 for the simulations is obtained. Thus vector radiative transfer causes a small but distinct improvement of the retrieval results.

To enhance the reliability of this finding, more validation sites have to be considered. However, to detect changes of less than 0.7 % in our retrieval product for different stations, we have to correct again for individual biases per station. For this purpose we consider validation points where the difference between using a scalar or a vector radiative transfer model $\Delta_{sca} - \Delta_{vect}$ is less than ±0.1 % and assume that for these cases the error is dominated by a bias, which does not depend on the particular radiative transfer solver. Subsequently, the mean bias of this subset is used to correct the entire validation set for the particular station. Finally, in Fig. 17, we consider the retrieval error

AMTD
8, 4917–4971, 2015

Δ_{ret} as a function of $\Delta_{sca} - \Delta_{vect}$. The figure shows a clear correlation between the differences $\Delta_{sca} - \Delta_{vect}$ and the validation errors Δ_{ret}. For scalar radiative transfer, the differences $\Delta_{sca} - \Delta_{vect}$ are mapped nearly one-to-one to corresponding errors of the validation. The use of a vector radiative transfer model thus represents an improvement of the validation dataset. For $\Delta_{sca} - \Delta_{vect} > 0.4\,\%$, the statistics become poor due to the fact that most validation sites are situated at latitudes larger than 50° N. Because of the sun-synchronous orbit of MetOp, this causes an asymmetric distribution of scattering angles in our dataset, which might explain the larger values of Δ_{ret} for $\Delta_{sca} - \Delta_{vect} > 0.4\,\%$. Conluding on the need of vector radiative transfer to retrieve total ozone columns from the 325–335 nm UV spectral window, the induced error of less than 0.7 %, using scalar radiative transfer, has to be viewed in the context of uncertainty requirements for this data product. For example for the future Sentinel-5 mission, an uncertainty of less then 3–5 % is required on the total ozone column product (Ingmann et al., 2012). In this context, we conclude that the use of a scalar radiative transfer solver is justified.

Because instrument degradation in the UV (e.g. GOME and SCIAMACHY) is a known issue, we investigate the influence of the scan angle degradation with time on the retrieved total ozone columns and omit the wavelength dependent degradation since it is small across the 325–335 nm fitting window. To do so, we perform a validation of retrieved total ozone columns calculated from GOME-2 measurements without and with the degradation correction described in Sect. 3 for a subset of collocated ground stations. The subset comprises the stations Ankara, Churchill (Brewer MKII.026), De Bilt, Edmonton (Brewer MKII.055), Hohenpeissenberg, Hong Kong Observatory, Izaña, Naha, and Paramaribo, and is chosen such that it represents different instruments and latitudes and it provides good data coverage for every single station in the investigated period. Figure 18 (top panel) shows an improvement in the validation in the last third of the time series, covering the period from September 2009 to December 2010, of $\Delta_{ret} \sim 0.5\,\%$ when the degradation correction is applied (red bars). Attributed to our approach of determining the degradation, no difference between retrievals with and without degradation correction is seen in 2007, since this year serves as reference as

AMTD
8, 4917–4971, 2015

discussed earlier. Therefore, δI_{deg} is zero in 2007 in the middle panel, which shows the mean radiometric degradation averaged over the corresponding two-month bin in the time series. The biases seen in the top panel show more variation which might relate to the choice of the validation sites, their instrumentation and the data coverage over the period under investigation, shown in the lower panel of the figure. However, in the context of biases of 0.6 % between Brewer and Dobson instruments (Staehelin et al., 2003) and 2 % between SAOZ and both, Brewer and Dobson instruments (Van Roozendael et al., 1998), the biases, that we report, are close to or within the limit of the validation. Concluding, the impact of degradation on the total ozone column is in the order of −0.5 % in the last part of the considered four-year period and has been corrected for. To investigate the scan angle dependency of the degradation and its influence on the retrieved product, we aggregate the dataset into six month bins of east and west pixels by dividing between eastwards (pixel index 2–12) and westwards (pixel index 13–24) scans in order to obtain meaningful statistics. Figure 19 shows that the retrieval error increases faster for the uncorrected western pixels (light blue) than for the eastern pixels (dark blue). Comparing the uncorrected retrievals with their corrected counterpart, western pixels in orange and eastern pixels in brown, this becomes even more obvious. Furthermore, the improvement by correcting degradation for the west pixels is in the order of $\Delta_{ret} \sim 0.5$ %, while the correction has a smaller effect for the east pixels. The spurious features seen here in the beginning of the time series are of the same origin as in Fig. 18. Because these errors already occur in the beginning of the time series, especially the difference between west and east pixels may hint at a radiometric calibration bias of the eastward pixels. From Fig. 19 we conclude that applying the degradation correction to the west pixels improves the validation from $\Delta_{ret} = -1.3$ % to $\Delta_{ret} = -0.6$ % at the end of the investigated four-year period, while the correction of the east pixels has a smaller effect.

Overall, with the western pixels being subject to stronger degradation and the continuation of the overall instrument degradation, we see a trend of an increasing bias Δ_{ret} starting in the last third of the investigated period. Hence, the application of the degra-

AMTD
8, 4917–4971, 2015

dation correction improves the validation in that interval and it is expected to become even more important for the ongoing mission beyond the period that we investigated.

5 Conclusions

In this paper, we presented an extensive sensitivity study of retrieved total ozone columns from clear sky GOME-2 measurements with respect to the choice of the scaling ozone profile, instrument degradation, cloudiness, topography, the approximation of Earth's sphericity, and the choice of the radiative transfer solver. We used a profile scaling approach and calculated total column averaging kernels for every retrieval in an analytical manner following the method of Borsdorff et al. (2014).

To mitigate the effect of instrument degradation, we determined a scan angle dependent degradation for the period under investigation solely based on GOME-2 measurements that are referenced to the corresponding day in 2007, which is also the first year of the mission. To do so, we assumed that the mean reflectance does not change with time for clear sky atmospheres for certain regions in the same period of the year, i.e. the same albedo and observation geometry. For the eastern pixels we found a degradation of about 3–4 %, while for the western pixels the degradation is up to 9.5 % at the end of the 4.5 year period. Based on these findings we corrected the GOME-2 measurements in the period 2008–2011.

We discussed regularization aspects of the inversion of a profile scaling approach and evaluated the use of the total column averaging kernel for a proper interpretation of the GOME-2 data product. When the null space is accounted for in the validation, the dependence on the reference scaling profile reduces significantly, e.g. for Naha to $\Delta_{ret} = -0.2\,\%$ instead of $\Delta_{ret} = -2.6\,\%$ (using the ozone profile of US standard atmosphere a reference) or $\Delta_{ret} = -0.8\,\%$ (using climatological ozone profiles from Fortuin and Kelder, 1998 as reference). When the ozone profile, serving as reference scaling profile, is used as well in the validation, the null space diminishes by definition. Here, we used ozonesonde profiles as best a priori knowledge of the reference profile and

AMTD
8, 4917–4971, 2015

subsequently in the validation, to demonstrate this effect. Thus, applying the total column averaging kernel allows us to focus on the information on the total ozone column in the GOME-2 measurement and makes the retrieval product less dependent on a priori knowledge of the vertical ozone distribution. In particular, for applications like the assimilation of the retrieved ozone column in a global or a regional model this presents a clear advantage, because the dependency of the GOME-2 product on a priori knowledge is reduced. In this study we applied this method in the validation of GOME-2 total ozone columns collocated with 647 measurements at 36 ground-based stations and found a global bias of 0.1 % with a SD of 2.5 %. Differences in elevation between the GOME-2 ground pixel and the validation site are accounted for, since they can introduce significant biases, for example for Izaña (−1.8 %) and Mauna Loa (−3.5 %).

To study the impact of clouds on the quality of the validation, we defined the cloudiness parameter η_{cld} as a product of cloud fraction and a cloud top height, normalized to a reference height of 10 km. Both, cloud fraction and cloud top height are retrieved with the FRESCO cloud algorithm (Wang et al., 2008). We proposed a cloud filtering with $\eta_{\mathrm{cld}} < 0.1$, which limits the introduced error due to clouds to $\Delta_{\mathrm{ret}} \leq -0.2$ %, while for larger values of $\eta_{\mathrm{cld}}\Delta_{\mathrm{ret}}$ increased from −1 to about −3 %. Another important key parameter is the representation of Earth's sphericity, and connected to that the influence of the solar zenith angle on the retrieval error. We investigated three approximations: (1) plane parallel assumption, (2) air mass correction by Kasten and Young (1989), and (3) the pseudo-spherical approximation by Walter et al. (2004), and found the smallest biases at large solar zenith angles ($\theta > 60^{\circ}$) for the pseudo-spherical approximation ranging from 2 to −1 %. Comparing the solar zenith angle dependence for a subset of retrievals, using the pseudo-spherical approximation, we found a generally higher solar zenith angle dependence for Dobson spectrometers than for Brewer instruments. For example, for the measurement site in Praha, which is equipped with both instruments, we found a remarkable dependence of about 1 % per 10° solar zenith angle for the Dobson instrument, compared to 0.1 % per 10° for the Brewer instrument. A more thorough study is needed, including collocations of different instruments at several sites, to

AMTD
8, 4917–4971, 2015

further investigate and confirm this finding. The use of a scalar radiative transfer model introduces an error of maximum 0.7 %. This error should be weighed against the much lower computational cost. Moreover, given the context of the uncertainty requirements of the total ozone column product of less than 3–5 % for the Sentinel-5 mission (Ingmann et al., 2012), we conclude that using a scalar radiative transfer model is sufficient.

Because instrument degradation is a known issue, we investigated the influence on the retrieved total ozone columns. Application of the degradation correction contributed to an overall more constant performance of the retrieval within the period of four years. We found that the stronger and faster degradation of the western pixels is reflected in the retrieval errors which are more strongly affected compared to the retrieval errors of the slower and weaker degrading eastern pixels. The degradation correction shows a larger effect for the western pixels of $\Delta_{ret} \sim 0.5\,\%$ than for the eastern pixels at the end of the studied period. Next to the degradation, we saw already in the first year of the mission a performance asymmetry between east and west pixels, which hints at an initial calibration bias of the instrument. This aspect has to be adressed in a future study. Overall, the application of the degradation correction led to an overall more constant performance and for long-term monitoring of ozone, degradation correction is expected to become even more important for the ongoing mission beyond the period that we investigated.

In summary, we validated our retrieval with collocated ground-based total column and ozonesonde measurements and found a mean bias of 0.1 % with a SD of 2.5 %. The consequent use of the total column averaging kernel in the validation makes the GOME-2 total ozone column data interpretation less dependent on the a priori knowledge of the vertical distribution of ozone and focuses on the information that can be extracted from the measurements. A thorough study of our retrieval setup showed good performance for clear sky retrievals with maximum sensitivity to tropospheric ozone. However, to increase the number of retrievals the cloudiness criterion could be relaxed when we account for clouds in the retrieval. To do so, our retrieval setup could be extended by the O_2-A band to retrieve cloud optical thickness and cloud height. Fur-

AMTD
8, 4917–4971, 2015

thermore, our validation showed sufficient accuracy, when a scalar radiative transfer solver with a pseudo spherical atmospheric approximation is used. We demonstrated that the proposed instrument degradation correction works, but found hints to an initial calibration issue between east and west pixels that has to be adressed in another study.

Acknowledgements. Total ozone data as well as ozone profiles were extracted from the publicly available databases maintained by the World Ozone and Ultraviolet Radiation Data Centre (WOUDC, see www.woudc.org), the Network for the Detection of Atmospheric Composition Change (NDACC, see www.ndsc.ncep.noaa.gov), and the Southern Hemisphere ADditional OZonesondes group (SHADOZ, see http://croc.gsfc.nasa.gov/shadoz). ECMWF ERA-40 data used in this study have been acquired from the European Centre for Medium-Range Weather Forecasts data server (ECMWF, see http://apps.ecmwf.int/datasets/).

References

Antón, M., Loyola, D., López, M., Vilaplana, J. M., Bañón, M., Zimmer, W., and Serrano, A.: Comparison of GOME-2/MetOp total ozone data with Brewer spectroradiometer data over the Iberian Peninsula, Ann. Geophys., 27, 1377–1386, doi:10.5194/angeo-27-1377-2009, 2009. 4919

Basher, R. E.: Review of the Dobson spectrophotometer and its accuracy, WMO Ozone Report 13, World Meteorological Organization, Geneva, Switzerland, 1982. 4931

Basher, R. E.: Survey of WMO-sponsored Dobson spectrophotometer intercomparisons, WMO Ozone Report 19, World Meteorological Organization, Geneva, Switzerland, 1994. 4931

Beekmann, M., Ancellet, G., Mégie, G., Smit, H. G. J., and Kley, D.: Intercomparison campaign of vertical ozone profiles including electrochemical sondes of ECC and Brewer–Mast type and a ground-based UV-Differential Absoption Lidar, J. Atmos. Chem., 19, 259–288, 1994. 4930

Beekmann, M., Ancellet; G., Martin, D., C. Abonnel, C., Duverneuil, G., Eideliman, F., Bessemoulin, P., Fritz, N., and Gizard, E.: Intercomparison of tropospheric ozone profiles obtained by electrochemical sondes, a ground-based lidar, and an airborne UV-photometer, Atmos. Environ., 29, 1027–1042, 1995. 4930

AMTD
8, 4917–4971, 2015

Berrisford, P., Dee, D., Fielding, K., Fuentes, M., Kallberg, P., Kobayashi, S., and Uppala, S.: The ERA-Interim archive, Technical Report 1, European Centre for Medium-Range Weather Forecasts, Reading, UK, 2009 4928

Bhartia, P. K. and Wellemayer, C. W.: TOMS v8 algorithm theoretical basis document, Technical Report, Greenbelt, Maryland, NASA, 2004. 4919

Bhartia, P. K., McPeters, R. D., Mateer, C. L., Flynn, L. E., and Wellemeyer, C.: Algorithm for the estimation of vertical ozone profile from the backscattered ultraviolet (BUV) technique, J. Geophys. Res., 101, 18793–18806, 1996. 4919

Borsdorff, T., Hasekamp, O. P., Wassmann, A., and Landgraf, J.: Insights into Tikhonov regularization: application to trace gas column retrieval and the efficient calculation of total column averaging kernels, Atmos. Meas. Tech., 7, 523–535, doi:10.5194/amt-7-523-2014, 2014. 4919, 4920, 4925, 4926, 4941

Bovensman, H., Burrows, J. P., Buchwitz, M., Frerick, J., Noël, S., Rozanov, V. V., Chance, K. V., and Goede, A. P. H.: SCIAMACHY: mission objectives and measurement modes, J. Atmos. Sci., 56, 127–150, doi:10.1175/1520-0469(1999)056<0127:SMOAMM>2.0.CO;2, 1999. 4919

Brion, J., Chakir, A., Daumont, D., Malicet, J., and Parisse, C.: High-resolution laboratory absorption cross section of O_3, Temperature effect, Chem. Phys. Lett., 213, 610–612, 1993. 4923

Bucholtz, A.: Rayleigh-Scattering calculations for the terrestrial atmosphere, Appl. Optics, 34, 2765–2773, 1995. 4923

Burrows, J., Weber, M., Buchwitz, M., Rozanov, V., Ladstätter-Weißenmayer, A., Richter, A., DeBeek, R., Hoogen, R., Bramstedt, K., Eichmann, K.-U., Eisinger, M., and Perner, D.: The Global Ozone Monitoring Experiment (GOME): mission concept and first scientific results, J. Atmos. Sci., 56, 151–175, 1999. 4919

Cai, Z., Liu, Y., Liu, X., Chance, K., Nowlan, C. R., Lang, R., Munro, R., and Suleiman, R.: Characterization and correction of Global Ozone Monitoring Experiment 2 ultraviolet measurements and application to ozone profile retrievals, J. Geophys. Res., 117, D07305, doi:10.1029/2011JD017096, 2012. 4920, 4928

Coldewey-Egbers, M., Weber, M., Lamsal, L. N., de Beek, R., Buchwitz, M., and Burrows, J. P.: Total ozone retrieval from GOME UV spectral data using the weighting function DOAS approach, Atmos. Chem. Phys., 5, 1015–1025, doi:10.5194/acp-5-1015-2005, 2005. 4919

AMTD
8, 4917–4971, 2015

Eskes, H. J., van der A, R. J., Brinksma, E. J., Veefkind, J. P., de Haan, J. F., and Valks, P. J. M.: Retrieval and validation of ozone columns derived from measurements of SCIAMACHY on Envisat, Atmos. Chem. Phys. Discuss., 5, 4429–4475, doi:10.5194/acpd-5-4429-2005, 2005. 4919

Farr, T. G., Rosen, P. A., Caro, E., Crippen, R., Duren, R., Hensley, S., Kobrick, M., Paller, M., Rodriguez, E., Roth, L., Seal, D., Shaffer, S., Shimada, J., Umland, J., Werner, M., Oskin, M., Burbank, D., and Alsdorf, D.: The Shuttle Radar Topography Mission, Rev. Geophys., 45, doi:10.1029/2005RG000183, 2007. 4930

Fioletov, V. E., Kerr, J. B., McElroy, C. T., Wardle, D. I., Savastiouk, V., and Grajnar, T. S.: The Brewer reference triad, Geophys. Res. Lett., 32, L20805, doi:10.1029/2005GL024244, 2005. 4931

Fioletov, V. E., Tarasick, D. W., and Petropavlovskikh, I.: Estimating ozone variability and instrument uncertainties from SBUV/2, ozonesonde, Umkehr, and SAGE II measurements: short-term variations, J. Geophys. Res., 111, D02305, doi:10.1029/2005JD006340, 2006. 4930

Fioletov, V. E., Labow, G., Evans, R., Hare, E. W., Köhler, U., McElroy, C. T., Miyagawa, K., Redondas, A., Savastiouk, V., Shalamyansky, A. M., Staehelin, J., Vanicek, K., and Weber, M.: Performance of the ground-based total ozone network assessed using satellite data, J. Geophys. Res., 113, D14313, doi:10.1029/2008JD009809, 2008. 4931

Fortuin, J. P. F. and Kelder, H.: An ozone climatology based on ozonesondes and satellite measurements, J. Geophys. Res., 103, 31709–31734, 1998. 4927, 4930, 4934, 4935, 4941, 4951, 4953, 4959, 4960

Hasekamp, O. and Landgraf, J.: Ozone profile retrieval from backscattered ultraviolet radiances: the inverse problem solved by regularization, J. Geophys. Res., 106, 8077–8088, doi:10.1029/2000JD900692, 2001. 4923

Hasekamp, O. P. and Landgraf, J.: Linearization of vector radiative transfer with respect to aerosol properties and its use in satellite remote sensing, J. Geophys. Res., 110, D04203, doi:10.1029/2004JD005260, 2005. 4923

Hoogen, R., Rozanov, V., and Burrows, J.: Ozone profiles from GOME satellite data: algorithm description and first validation, J. Geophys. Res., 104, 8263–8280, 1999. 4923

Ingmann, P., Veihelmann, B., Langen, J., Lamarre, D., Stark, H., and Courrèges-Lacoste, G. B.: Requirements for the GMES Atmosphere Service and ESA's implementation concept:

AMTD
8, 4917–4971, 2015

Sentinels-4/-5 and -5p, Remote Sens. Environ., 120, 58–59, doi:10.1016/j.rse.2012.01.023, 2012. 4939, 4943
Kasten, F. and Young, T.: Revised optical air mass tables and approximation formula, Appl. Optics, 28, 4375, doi:10.1364/AO.28.004735, 1989. 4936, 4942, 4963
Kerr, J. B., Fast, H., McElroy, C. T., Oltmans, S. J., Lathrop, J. A., Kyrö, E., Paukkunen, A., Claude, H., Köhler, U., Sreedharan, C. R., Takao, T., and Tsukagoshi, Y.: The 1991 WMO international ozonesonde intercomparison at Vanscoy, Canada, Atmos. Ocean, 32, 685–716, doi:10.1080/07055900.1994.9649518, 1994. 4930
Kerr, J. B., McElroy, C. T., and Wardle, D. W.: The Brewer instrument calibration center 1984–1996, in: Atmospheric Ozone: Proceedings of the XVIII Ozone Symposium, Parco Sci., and Tecnologico D' Abruzzo, L'Aquila, Italy, 915–918, 1997. 4931
Komhyr, W. D., Grass, R. D., and Leonard, R. K.: Dobson spectrophotometer 83: a standard for total ozone measurements 1963–1987, J. Geophys. Res., 94, 9847–9861, 1989. 4931
Koukouli, M. E., Balis, D. S., Loyola, D., Valks, P., Zimmer, W., Hao, N., Lambert, J.-C., Van Roozendael, M., Lerot, C., and Spurr, R. J. D.: Geophysical validation and long-term consistency between GOME-2/MetOp-A total ozone column and measurements from the sensors GOME/ERS-2, SCIAMACHY/ENVISAT and OMI/Aura, Atmos. Meas. Tech., 5, 2169–2181, doi:10.5194/amt-5-2169-2012, 2012. 4920
Krijger, J. M., Aben, I., and Landgraf, J.: CHEOPS-GOME: WP2.1: study of instrument degradation, Report SRON-EOS/RP/05-018, European Space Agency, Paris, France, 2005. 4920
Landgraf, J., Hasekamp, O. P., Box, M. A., and Trautmann, T.: A linearized radiative transfer model for ozone profile retrieval using the analytical forward-adjoint pertubation theory approach, J. Geophys. Res., 106, 27291–27305, 2001. 4923
Landgraf, J., Hasekamp, O. P., van Deelen, R., and Aben, I.: Rotational Raman scattering of polarized light in the Earth atmosphere: a vector radiative transfer model using the radiative transfer perturbation theory approach, J. Quant. Spectrosc. Ra., 87, 399–433, doi:10.1016/j.jqsrt.2004.03.013, 2004. 4923
Lerot, C., van Roozendael, M., Lambert, J.-C., Granville, J., van Gent, J., Loyola, D., and Spurr, R.: The GODFIT algorithm: a direct fitting approach to improve the accuracy of total ozone measurementsfrom GOME, Int. J. Remote Sens., 31, 543–550, doi:10.1080/01431160902893576, 2010. 4919, 4924
Lerot, C., van Roozendael, M., Spurr, R., Loyola, D., Coldewey-Egbers, M., Kochenova, S., van Gent, J., Koukouli, M., Balis, D., Lambert, J.-C., Granville, J., and Zehner, C.: Homogenized

AMTD
8, 4917–4971, 2015

total ozone data records from the European sensors GOME/ERS-2, SCIAMACHY/Envisat, and GOME-2/MetOp-A, J. Geophys. Res., 119, 1639–1662, doi:10.1002/2013JD020831, 2014. 4919, 4923, 4927

Levelt, P. F., van den Oord, G. H. J., Dobber, M. R., Mälkki, A., Visser, H., de Vries, J., Stammes, P., Lundell, J. O. V., and Saari, H.: The ozone monitoring instrument, IEEE T. Geosci. Remote, 44, 1093–1101, doi:10.1109/TGRS.2006.872333, 2006. 4919

Liu, X., Chance, K., and Kurosu, T. P.: Improved ozone profile retrievals from GOME data with degradation correction in reflectance, Atmos. Chem. Phys., 7, 1575–1583, doi:10.5194/acp-7-1575-2007, 2007. 4920, 4929

Loyola, D. G., Koukouli, M. E., Valks, P., Balis, D. S., Hao, N., Van Roozendael, M., Spurr, R. J. D., Zimmer, W., Kiemle, S., Lerot, C., and Lambert, J.-C.: The GOME-2 total column ozone product: retrieval algorithm and ground-based validation, J. Geophys. Res., 116, D07302, doi:10.1029/2010JD014675, 2011. 4919, 4920

NOAA: US Standard Atmosphere, 1976, Technical Report NOAA-S/T76-1562, National Oceanic and Atmospheric Administration, US Gov. Printing Office, Washington, DC, 1976. 4927, 4967

Nowlan, C. R., Liu, X., Chance, K., Cai, Z., Kurosu, T. P., Lee, C., and Martin, R. V.: Retrievals of sufur dioxide from the Global Ozone Monitoring Experiment 2 (GOME-2) using an optimal estimation approach: algorithm and initial validation, J. Geophys. Res., 116, D18301, doi:10.1029/2011JD015808, 2011. 4920

Rodgers, C. D.: Inverse Methods for Atmospheres: Theory and Practice, vol. 2, World Scientific, Singapore, New Jersey, London, Hong Kong, 2000. 4926

Schepers, D., aan de Brugh, J. M. J., Hahne, Ph., Butz, A., Hasekamp, O. P., and Landgraf, J.: LINTRAN v2.0: a linearised vector radiative transfer model for efficient simulation of satellite-born nadir-viewing reflection measurements of cloudy atmospheres, J. Quant. Spectrosc. Ra., 149, 347–359, doi:10.1016/j.jqsrt.2014.08.019, 2014. 4923

Smit, H. G. J. and Kley, D.: JOSIE: The 1996 WMO international intercomparison of ozonesondes under quasi flight conditions in the environmental simulation chamber at Jülich, WMO Global Atmosphere Watch report series, No. 130 (Technical Document No. 926), World Meteorological Organization, Geneva, Switzerland, 1998. 4930

Staehelin, J., Kerr, J., Evans, R., and Vanicek, K.: Comparison of total ozone measurements of Dobson and Brewer spectrophotometers and recommended transfer functions, Report WMO TD 1147, World Meteorological Organization, Geneval, Switzerland, 2003. 4931, 4940

AMTD
8, 4917–4971, 2015

Thompson, A. M., Witte, J. C., Smit, H. G. J., Oltmans, S. J., Johnson, B. J., Kirchhoff, V. W. J. H., and Schmidlin, F. J.: Southern Hemisphere Additional Ozonesondes (SHADOZ) 1998–2004 tropical ozone climatology: 3. Instrumentation, station-to-station variability, and evaluation with simulated flight profiles, J. Geophys. Res., 112, D03304, doi:10.1029/2005JD007042, 2007. 4931

Tilstra, L. G., Tuinder, O. N. E., and Stammes, P.: A new method for in-flight degradation correction of GOME-2 Earth reflectance measurements, with application to the absorbing aerosol index, Porceedings of the EUMETSAT Satellite Conference, 2–7 September 2012, Sopot, Poland, 2012. 4930

Valks, P., Loyola, D., Hao, N., Hedelt, P., Slijkhuis, S., and Grossi, M.: Algorithm theoretical basis document for GOME-2 total column products of ozone, tropospheric ozone, NO_2, tropospheric NO_2, BrO, SO_2, H_2O, OClO and cloud properties Report DLR/GOME-2/ATBD/01, Deutsches Zentrum für Luft und Raumfahrt e.V. – DLR, Oberpfaffenhofen, Germany, 2013. 4919

van Deelen, R., Landgraf, J., and Aben, I.: Multiple elastic and inelastic light scattering in the Earth's atmosphere: a doubling-adding method to include rotational Raman scattering by air, J. Quant. Spectrosc. Ra., 95, 309–330, doi:10.1016/j.jqsrt.2004.11.002, 2005. 4923

van Deelen, R., Hasekamp, O. P., and Landgraf, J.: Accurate modeling of spectral fine-structure in Earth radiance spectra measured with the Global Ozone Monitoring Experiment, Appl. Optics, 46, 243–252, doi:10.1364/AO.46.000243, 2007.

van der A, R. J., van Oss, R. F., Piters, A. J. M., Fortuin, J. P. F., Meijer, Y. F., and Kelder, H. M.: Ozone profile retrieval from recalibrated Global Ozone Monitoring Experiment data, J. Geophys. Res., 107, 4239, doi:10.1029/2001JD000696, 2002. 4920

Van Roozendael, M., Peeters, P., Roscoe, H. K., De Backer, H., Jones, A. E., Bartlett, L., Vaughan, G., Goutail, F., Pommereau, J.-P., Kyrö, E., Wahlstrom, C., Braathen, G., and Simon, P. C.: Validation of ground-based visible measurements of total ozone by comparison with Dobson and Brewer spectrophotometers, J. Atmos. Chem., 29, 55–83, 1998. 4931, 4940

Van Roozendael, M., Loyola, D., Spurr, R., Balis, D., Lambert, J.-C., Livschitz, Y., Valks, P., Ruppert. T., Kenter, P., Fayt, C., and Zehner, C.: Ten years of GOME/ERS-2 total ozone data – the new GOME data processor (GDP) version 4: 1. Algorithm description, J. Geophys. Res., 111, D14311, doi:10.1029/2005JD006375, 2006. 4919

AMTD
8, 4917–4971, 2015

van Soest, G., Tilstra, L. G., and Stammes, P.: Large-scale validation of SCIAMACHY reflectance in the ultraviolet, Atmos. Chem. Phys., 5, 2171–2180, doi:10.5194/acp-5-2171-2005, 2005. 4920

Veefkind, J. P., De Haan, J., Brinksma, E., Kroon, M., and Levelt, P.: Total ozone from the Ozone Monitoring Instrument (OMI) using the OMI-DOAS technique, IEEE T. Geosci. Remote, 44, 1239–1244, doi:10.1109/TGRS.2006.871204, 2004. 4919

Walter, H. H., Landgraf, J., and Hasekamp, O. P.: Linearization of a pseudo-spherical vector radiative transfer model, J. Quant. Spectrosc. Ra., 85, 251–283, doi:10.1016/S0022-4073(03)00228-0, 2004. 4923, 4936, 4942, 4963

Wang, P., Stammes, P., van der A, R., Pinardi, G., and van Roozendael, M.: FRESCO+: an improved O_2 A-band cloud retrieval algorithm for tropospheric trace gas retrievals, Atmos. Chem. Phys., 8, 6565–6576, doi:10.5194/acp-8-6565-2008, 2008. 4928, 4929, 4932, 4942

Weber, M., Lamsal, L. N., Coldewey-Egbers, M., Bramstedt, K., and Burrows, J. P.: Pole-to-pole validation of GOME WFDOAS total ozone with groundbased data, Atmos. Chem. Phys., 5, 1341–1355, doi:10.5194/acp-5-1341-2005, 2005. 4919

AMTD
8, 4917–4971, 2015

Table 1. Number of measurements N, biases b and error SD σ of the validation for each station. Dataset 1 comprises the results of the effective column comparison using ozonesonde profiles as reference and the filter criteria $\delta t < 15$ DU, $\delta r < 300$ km, $\chi^2 \leq 2$, and $\eta_{\mathrm{cld}} < 0.1$ are applied. Dataset 2 comprises the results used in Sect. 4.2. The reference profiles are taken from the climatology by Fortuin and Kelder (1998), and the filter criterion $\delta t < 30$ DU is relaxed, while the other remain as for dataset 1.

Station Name	Lat	Lon	Instrument	dataset 1			dataset 2		
				N	b [%]	σ [%]	N	b [%]	σ [%]
Alert	82.5° N	62.3° W	B-MKII.019	7	0.2	3.0	121	0.9	3.0
Eureka	80.1° N	86.2° W	B-MKV.069	13	−1.1	1.1	130	−0.7	2.4
Resolute	74.7° N	95.0° W	B-MKII.031	7	0.4	1.4	166	−0.4	3.3
Scoresbysund	70.5° N	22.0° W	SAOZ[a]	13	4.2	2.8	164	3.2	3.5
Lerwick	60.1° N	1.2° W	D-Beck.032	8	−0.3	2.2	85	0.1	2.6
Churchill	58.8° N	94.0° W	B-MKII.026	18	0.6	4.8	155	0.5	3.5
			B-MKIV.032	17	2.2	4.8	137	1.3	3.7
Edmonton	53.6° N	114.1° W	B-MKII.055	24	−0.9	2.0	290	−0.1	2.5
			B-MKIV.022	25	−0.5	3.0	236	−0.1	2.9
Goose Bay	53.3° N	60.4° W	B-MKII.018	15	0.7	2.7	209	0.7	2.5
Lindenberg	52.2° N	14.1° E	B-MKII.030	10	−0.1	2.7	96	−0.9	2.3
De Bilt	52.1° N	5.2° E	B-MKIII.189	17	−1.0	1.8	202	−1.3	1.8
Valentia Obs.	51.9° N	10.3° W	B-MKIV.088	10	−0.6	2.9	150	−0.5	2.2
Uccle	50.8° N	4.4° E	B-MKII.016	33	0.5	2.5	172	0.3	2.1
			B-MKIII.178	40	0.5	1.8	177	0.2	2.0
Praha	50.0° N	14.5° E	D-Beck.070	5	1.4	2.7	79	−0.7	2.3
			B-MKIII.184	6	0.0	2.0	207	−1.0	2.2
			B-MKIV.098	7	0.4	2.1	222	−0.9	2.4
Hohenpeissenberg	47.8° N	11.0° E	B-MKII.010	49	−0.6	1.9	215	−0.3	1.8
Egbert	44.2° N	79.8° W	B-MKII.015	26	0.2	2.8	274	0.2	3.5
OHP	43.9° N	5.7° E	D-Beck.085	9	−0.1	2.2	38	0.5	2.3
			SAOZ[a]	29	0.1	2.5	327	−0.0	2.5
Sapporo	43.1° N	141.3° E	D-Beck.126	15	−1.0	1.9	177	0.6	3.0
Madrid	40.5° N	3.6° W	B-MKIV.070	16	−0.8	2.9	184	−1.1	2.2
Boulder	40.1° N	105.3° W	D-Beck.082	22	1.1	2.5	161	0.8	2.9
Ankara	40.0° N	32.9° E	B-MKIII.188	11	−0.2	1.6	280	0.2	2.3
Tateno	36.1° N	140.1° E	D-Beck.125	14	1.9	2.7	145	1.0	3.1
Izaña	28.3° N	16.5° W	B-MKIII.157[a]	36	−0.6	1.4	342	0.2	1.7
Naha	26.2° N	127.7° E	D-Beck.127	47	0.1	1.7	409	−0.6	2.1
Hong Kong Obs.	22.3° N	114.2° E	B-MKIV.115	36	1.0	2.0	376	−1.2	1.8
Mauna Loa[b]	19.6° N	155.1° W	D-Beck.076	28	1.2	1.7	205	1.1	1.6
Paramaribo	5.8° N	55.2° W	B-MKIII.159	48	−0.3	1.1	482	−0.3	1.2
Sepang Airport	2.7° N	101.7° E	B-MKII.090	22	0.5	2.5	338	0.0	2.2

AMTD
8, 4917–4971, 2015

Table 1. Continued.

Station Name	Lat	Lon	Instrument	dataset 1			dataset 2		
				N	*b* [%]	σ [%]	*N*	*b* [%]	σ [%]
Samoa	14.3° S	170.6° W	D-Beck.042	–	–	–	33	0.9	1.7
Reunion Island	21.0° S	55.5° E	SAOZ[a]	58	0.4	1.7	620	0.0	1.5
Broadmeadows	37.7° S	145.0° E	D-Beck.115	26	−0.1	2.5	305	−1.1	4.0
Lauder	45.0° S	169.7° E	D-Beck.072	–	–	–	108	−1.1	4.2
Macquarie Island	54.5° S	159.0° E	D-Beck.006	5	0.5	2.8	71	−2.3	4.2
Ushuaia	54.9° S	68.3° W	D-Beck.131	–	–	–	71	1.2	3.4
Marambio	64.2° S	56.7° W	D-Beck.099	6	0.7	1.7	99	3.3	2.9
Dumont d'Urville	66.7° S	140.0° E	SAOZ[a]	9	0.3	3.8	216	1.6	4.2
Syowa	69.0° S	39.6° E	D-Beck.119	5	−1.0	2.8	56	−0.6	2.7
Global				647	0.1	2.5	6861	−0.1	2.7

[a] No observation mode was given, so all available data were used that meet the collocation criteria.
[b] In dataset 1 collocated ozonesondes from the station Hilo are used.

AMTD
8, 4917–4971, 2015

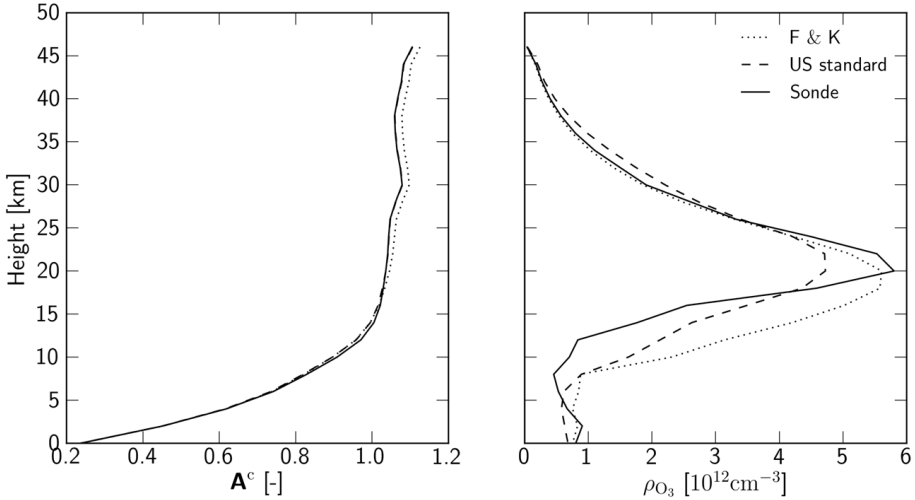

Figure 1. Left panel: total column averaging kernel using the ozone profile of the US standard atmosphere (dashed), from the climatology by Fortuin and Kelder (1998) (dotted), and the ozonesonde profile from 15 January 2009 over De Bilt, Netherlands (solid). The right panel shows the corresponding ozone profiles.

AMTD
8, 4917–4971, 2015

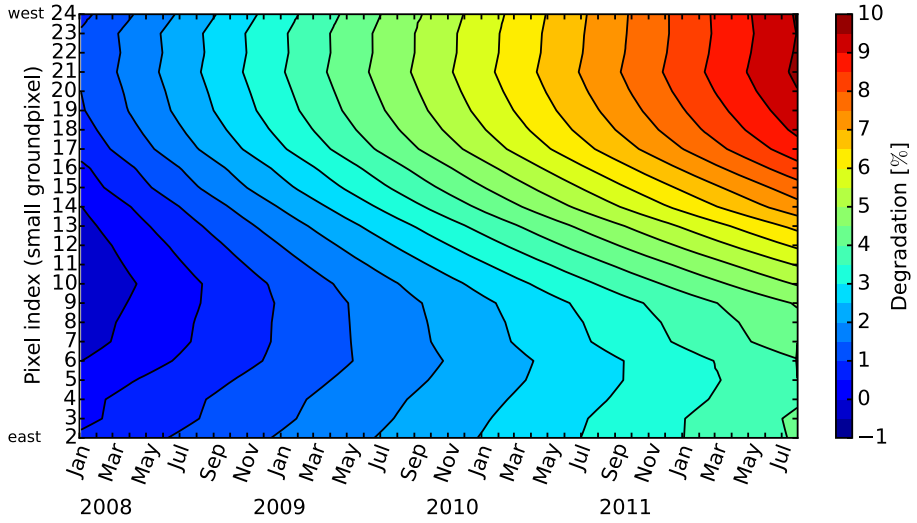

Figure 2. Degradation of globally averaged reflectances with respect to reference year 2007 per small ground pixel at 330 nm in the ozone fitting window (325–335 nm). Ground pixel 2 is the easternmost pixel of a scan and pixel 24 is the western pixel.

AMTD
8, 4917–4971, 2015

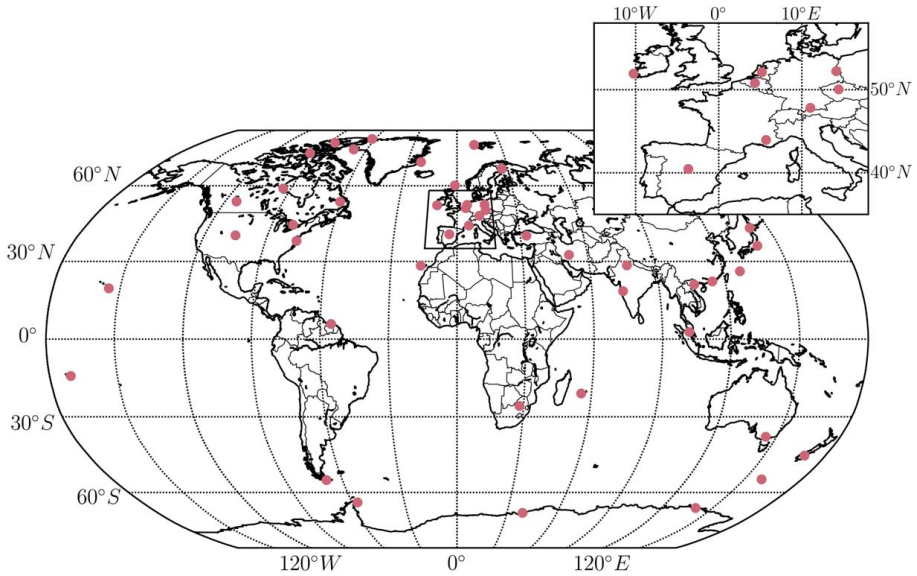

Figure 3. Map of validation stations with a zoom-in map of Western Europe, Central Europe, and Southern Europe. The outlines of the zoom-in map are shown on the global map in solid black lines. Each of the red dots depicts a validation station comprising both ozonesonde and ground-based data. Details of each station are given in Table 1.

AMTD
8, 4917–4971, 2015

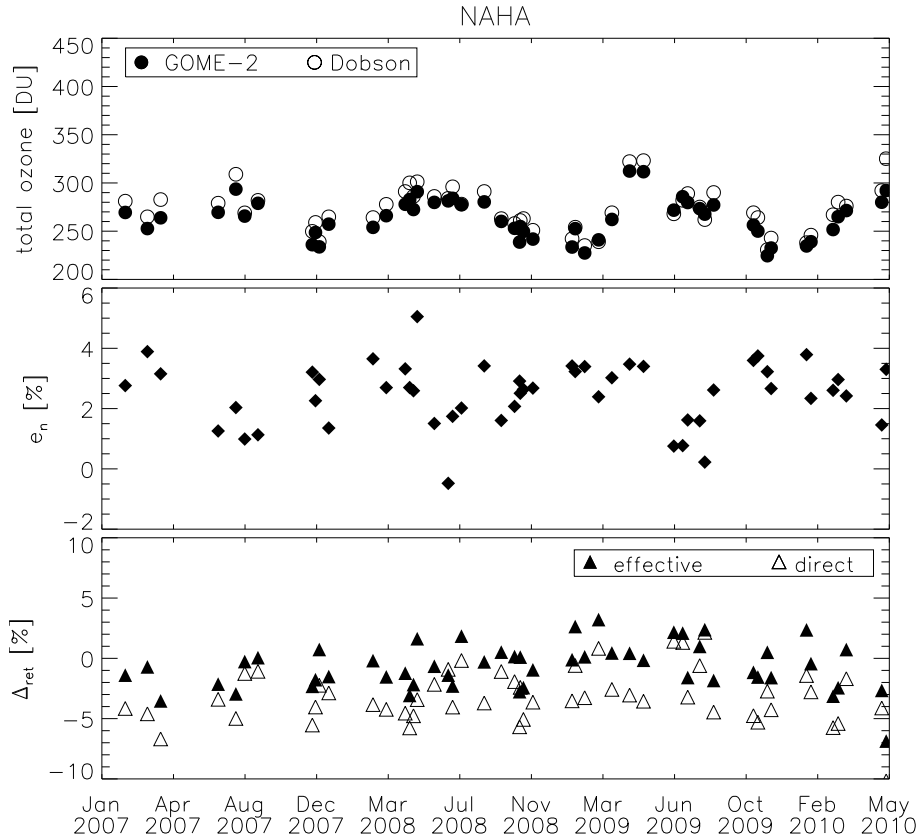

Figure 4. Time series of GOME-2 retrievals validated with ground-based Dobson direct sun measurements at Naha, Japan: (upper panel) retrieved GOME-2 total ozone column (filled circle) and the Dobson ground-based ozone column (open circle). (Middle panel) The null space contribution e_n. (Lower panel) The retrieval error for a direct comparison of the GOME-2 column with the Dobson column (open triangles) and for the effective column comparison accounting for the effective null space contribution e_n (Eq. 14) (filled triangles).

AMTD
8, 4917–4971, 2015

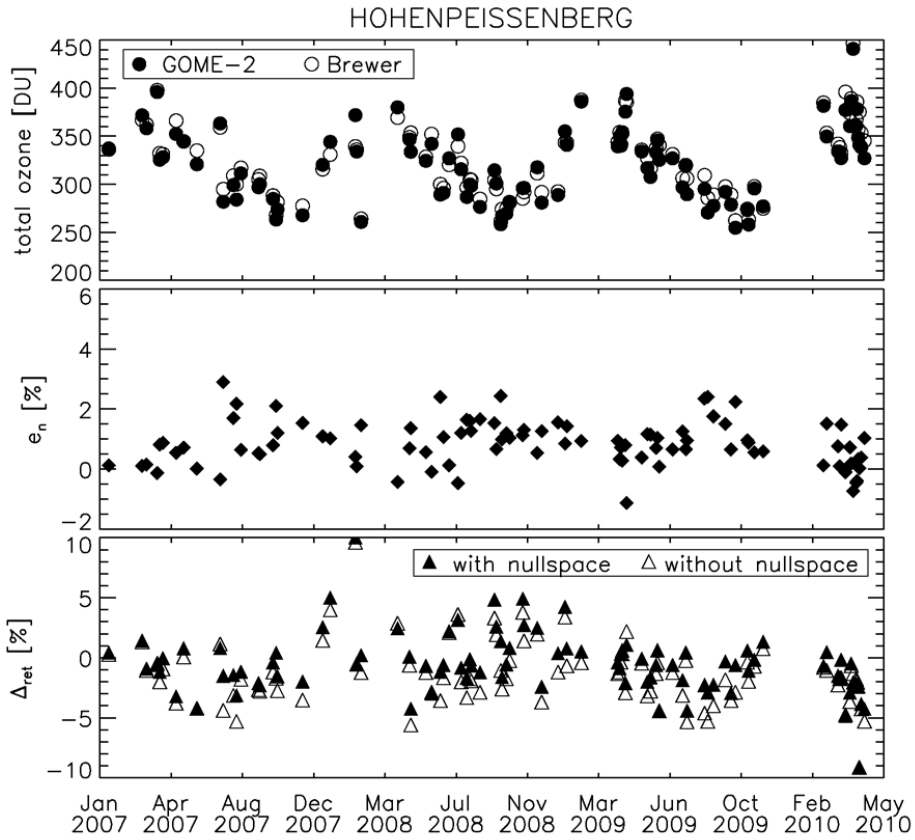

Figure 5. Time series of GOME-2 retrievals validated with ground-based Brewer direct sun measurements at Hohenpeissenberg, Germany: (upper panel) retrieved GOME-2 total ozone column (filled circle) and the Brewer ground-based ozone column (open circle). (Middle panel) The null space contribution e_n. (Lower panel) The retrieval error for a direct comparison of the GOME-2 column with the Brewer column (open triangles) and for the effective column comparison accounting for the effective null space contribution e_n (Eq. 14) (filled triangles).

AMTD
8, 4917–4971, 2015

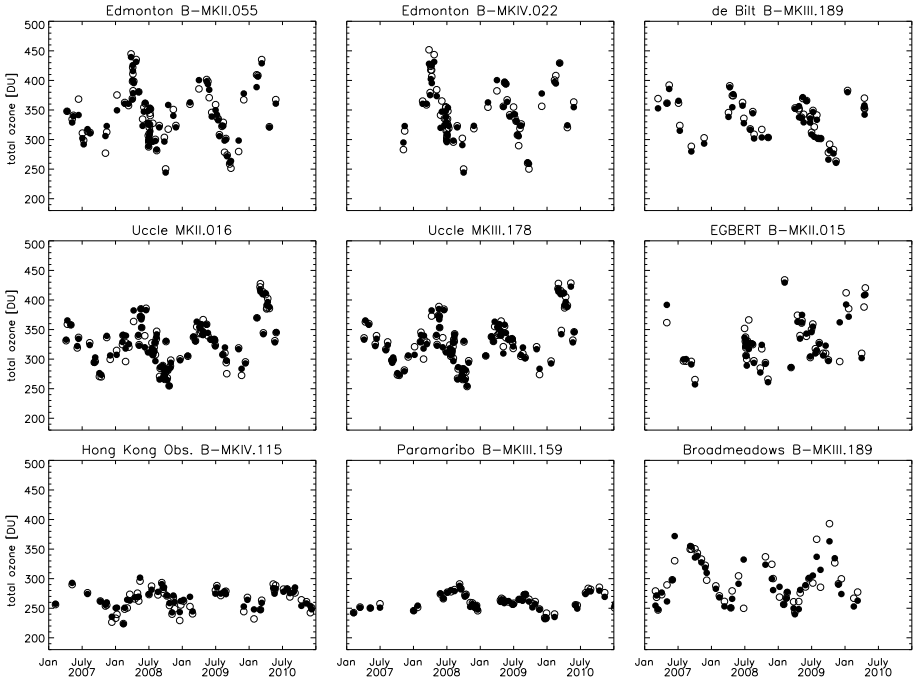

Figure 6. Time series of retrieved GOME-2 total ozone columns (filled circles) and collocated ground-based direct sun measurements (open circles) for stations with more than 15 spatiotemporal collocations. Details on instrumentation and geolocations of the measurement sites are given in Table 1.

AMTD
8, 4917–4971, 2015

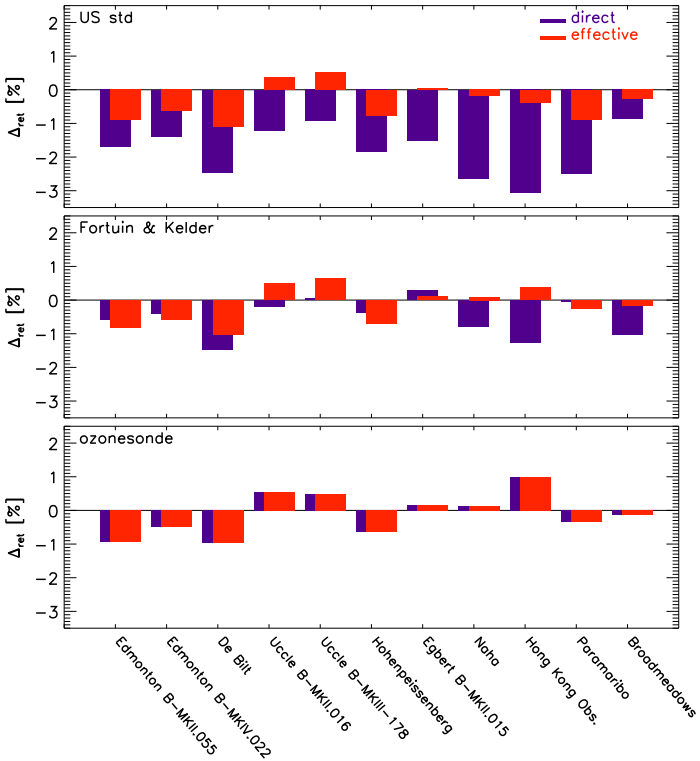

Figure 7. Mean error of the retrieved ozone column using different reference ozone profiles ρ_{ref}: (upper panel) adapted from the US standard atmosphere, (middle panel) from the ozone climatology of Fortuin and Kelder (1998), and (lower panel) collocated ozonesonde measurements. The red bars indicate the validation concept of the total column estimate including the total column averaging kernel and purple bars denote the direct comparison concept.

AMTD
8, 4917–4971, 2015

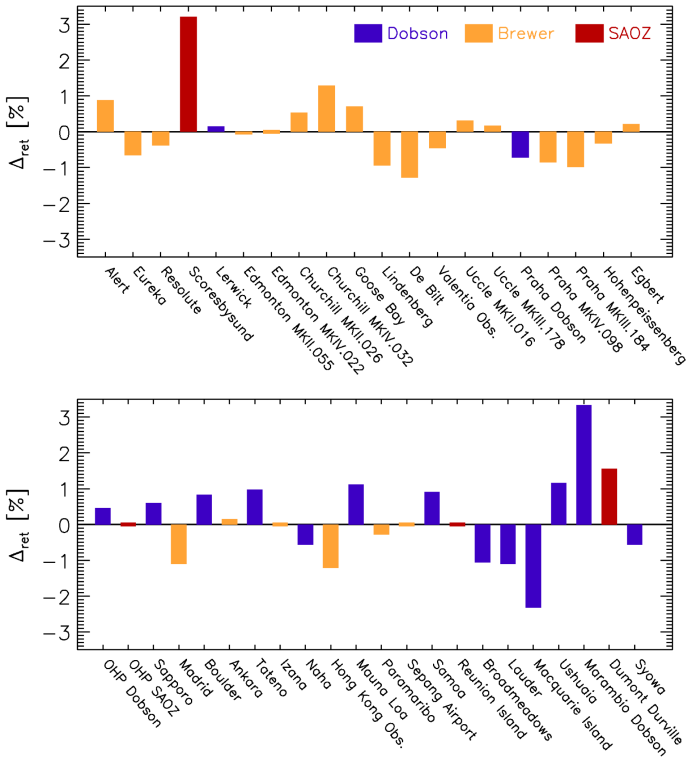

Figure 8. Retrieval bias using the ozone climatology of Fortuin and Kelder (1998) as reference profile to be scaled by the retrieval (dataset 2). Different colours of the bars denote different ground-based instruments used in the validation: Dobson (blue), Brewer (yellow), and SAOZ (red).

AMTD
8, 4917–4971, 2015

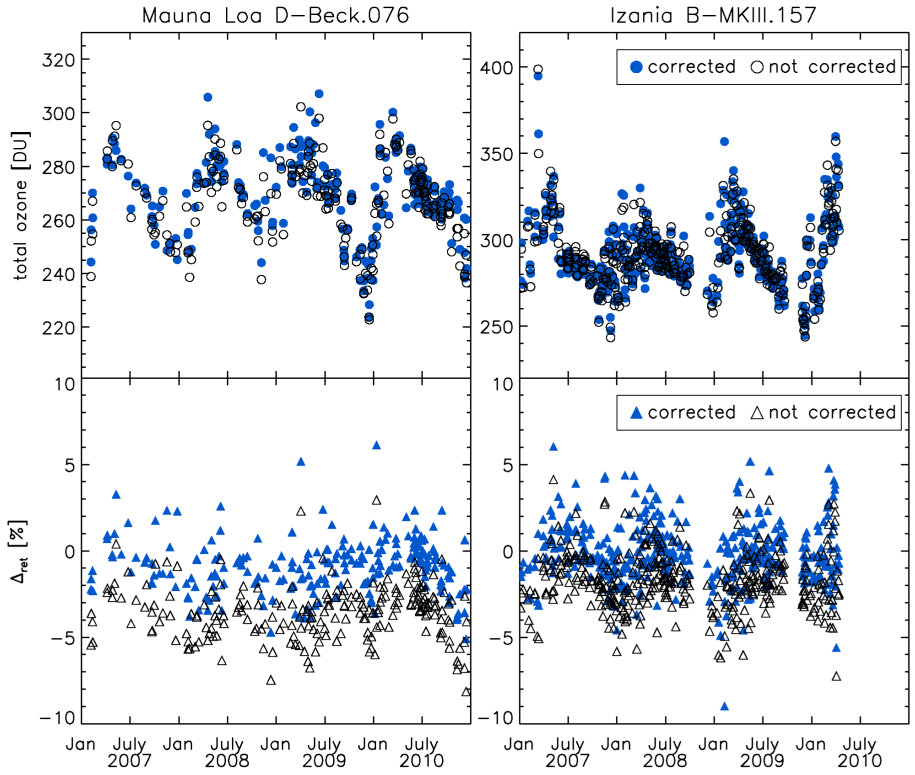

Figure 9. Time series of total ozone columns and the retrieval error for dataset 2. Upper panels: the retrieved ozone column (filled blue circles) using the elevation correction, and the ground-based measurements (open circles) for the sites Izaña and Mauna Loa. Lower panels: retrieval error accounting and not accounting for the elevation differences between satellite ground pixel and measurement site (filled blue and open triangles, respectively).

AMTD
8, 4917–4971, 2015

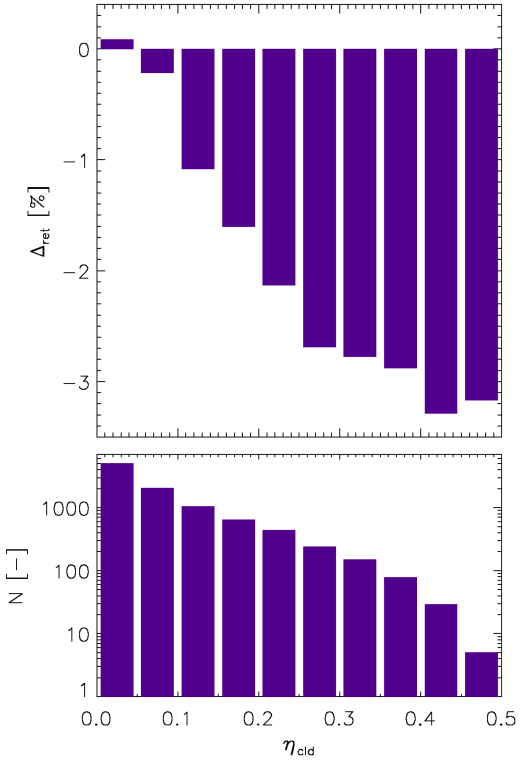

Figure 10. Mean retrieval error as function of the cloudiness parameter η_{cld} (Eq. 16) aggregated into bins of η_{cld} = 0.05. (Upper panel) The mean retrieval error in per cent. (Lower panel) Number of data points per bin of cloudiness. In total, the dataset comprises 9600 data points.

AMTD
8, 4917–4971, 2015

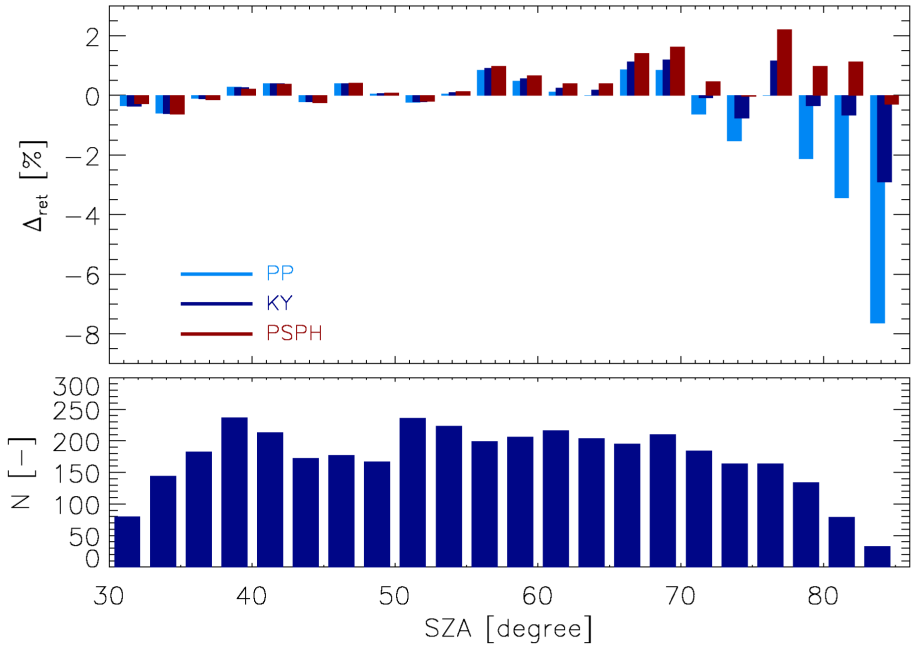

Figure 11. Mean ozone retrieval error as a function of solar zenith angle θ for different approximations of Earth's sphericity in the radiative transfer calculation. (Upper panel) The mean ozone retrieval error in per cent for the plane parallel approximation (PP, light plue), airmass correction of Kasten and Young (1989) (KY, dark blue), and pseudo-spherical approximation (Walter et al., 2004) (PSPH, red). (Lower panel) Number of data points per 2.5° bin of θ. The validation set comprises cloudfree measurements at Resolute, Churchill B-MKII.026, Edmonton B-MKII.055, Lindenberg, Macquarie Island, Dumont Durville, Goose Bay (see Table 1 for more details about the different sites). For each measurement site, the data are corrected for an overall bias for solar zenith angles $\theta < 55$.

AMTD
8, 4917–4971, 2015

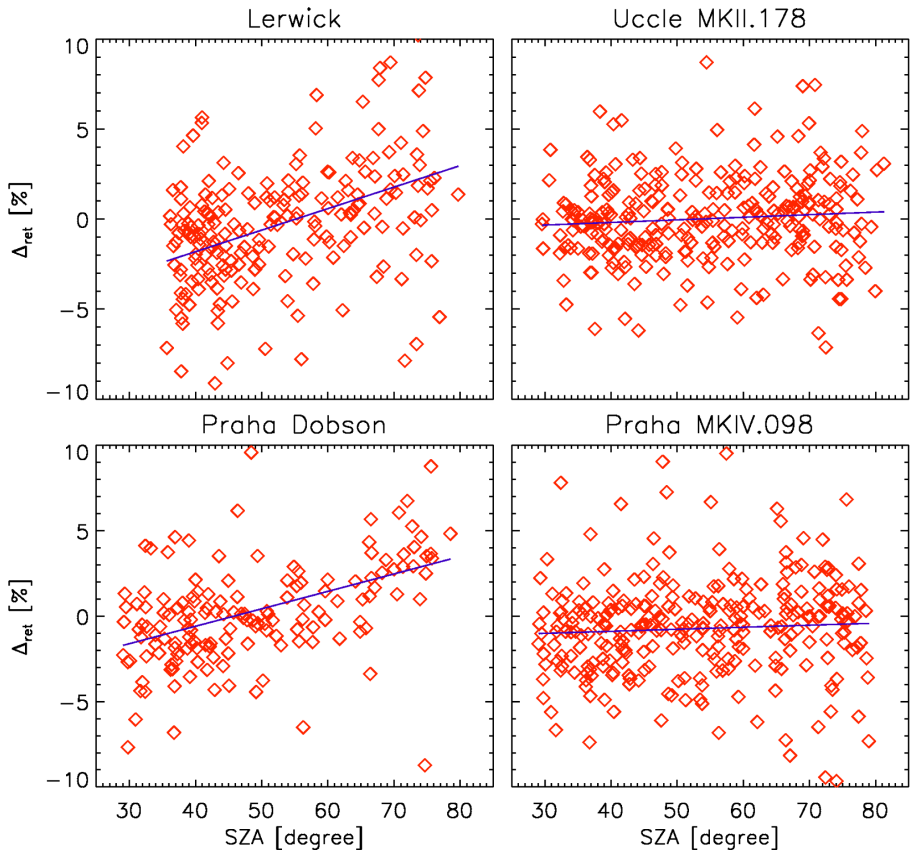

Figure 12. Retrieval error Δ_{ret} as function of solar zenith angle θ for Lerwick (upper left), Uccle B-MKII.178 (upper right), and Praha (Dobson, lower left, and B-MKIV.098 lower right). The blue lines are trends determined by linear regression.

AMTD
8, 4917–4971, 2015

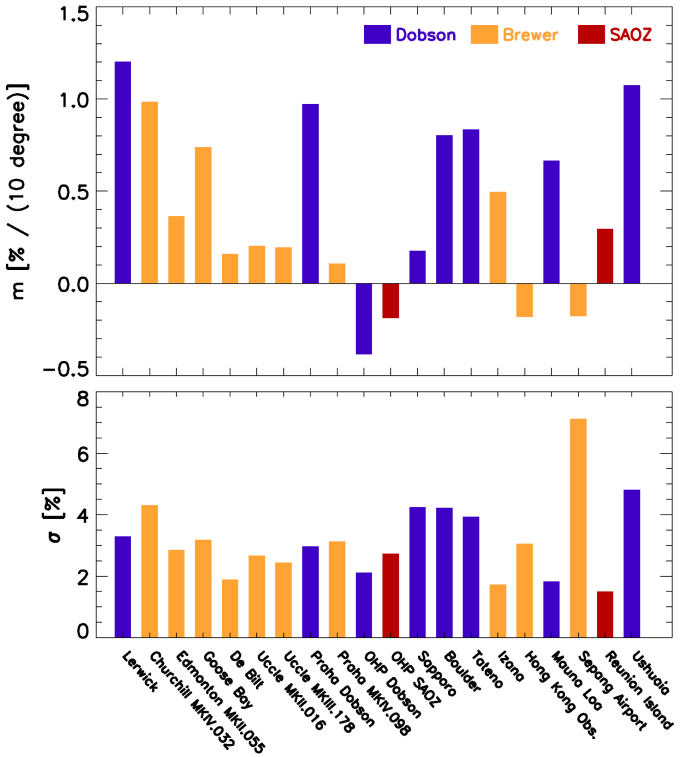

Figure 13. Dependence of the retrieval error Δ_{ret} on solar zenith angle θ, characterized by the slope of a linear regression through the data point per 10° solar zenith angle (upper panel, see also Fig. 12) and the SD around the linear regression (lower panel).

AMTD
8, 4917–4971, 2015

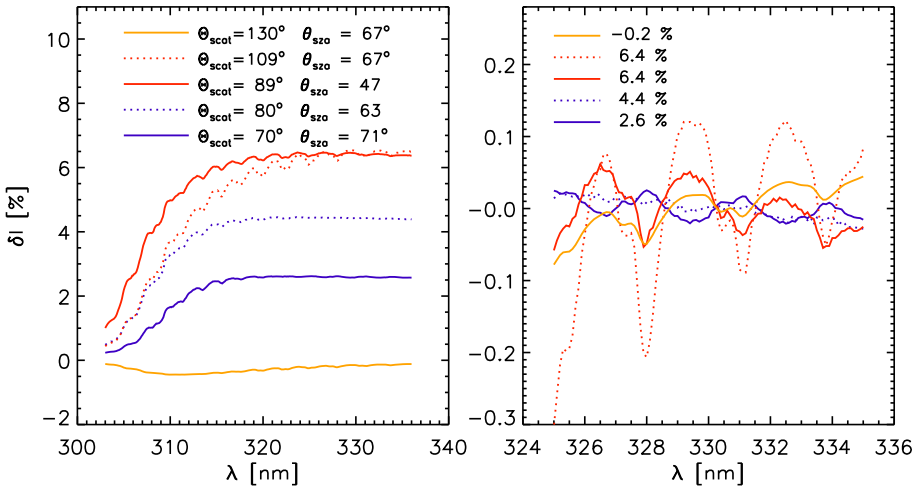

Figure 14. Relative error in the radiance simulation due to the scalar radiative transfer approximation for different scattering geometries. (Left) Relative radiance error $\delta I = (I_{scal} - I_{vec})/I_{vec}$ for different scattering angles Θ_{scat} and solar zenith angles θ. (Right panel) Same as right panel but zoom-in on retrieval window. The mean error for the indicated spectral window is subtracted and reported in the figure legend.

AMTD
8, 4917–4971, 2015

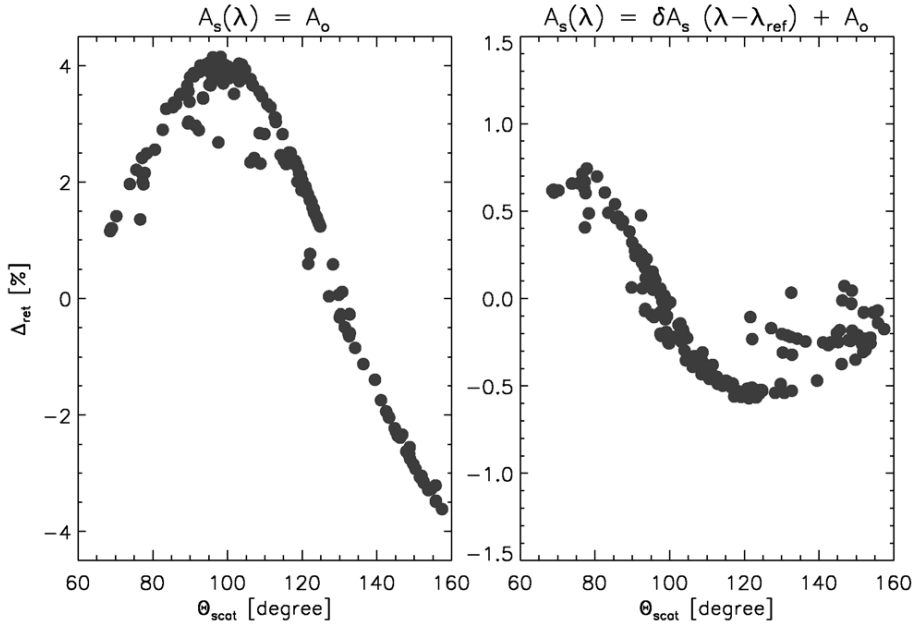

Figure 15. Ozone column error in the radiance simulation for solar and viewing geometries adapted from GOME-2 measurements of the Lerwick validation dataset. All measurements are simulated using a scalar radiative transfer model for clear sky conditions and the Lambertian surface albedo of 0.1 %. The atmospheric ozone abundance is taken from the US standard atmosphere NOAA (1976). The retrieval error is corrected for noise contributions. (Left panel) All fit parameters of our model including only a spectrally constant albedo. (Right) Same as left panel but retrieving a spectrally linear dependent albedo.

AMTD
8, 4917–4971, 2015

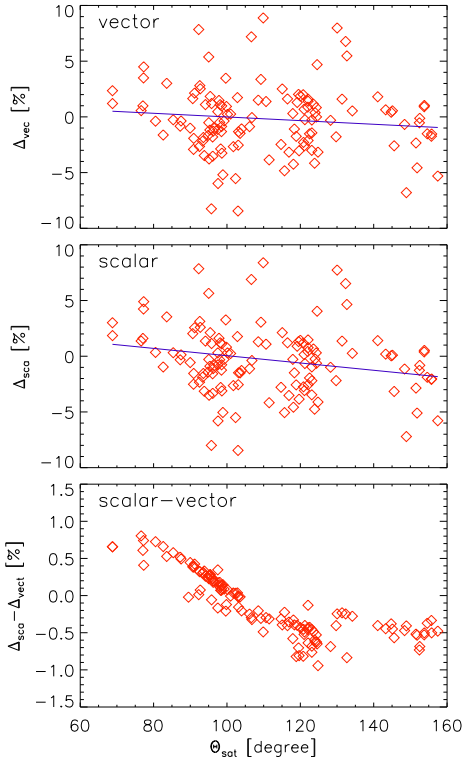

Figure 16. Total ozone column retrieval error Δ_{ret} as function of scattering angle Θ_{scat} in single scattering geometry. (Upper panel) For vector radiative transfer and (middle panel) for scalar radiative transfer. (Lower panel) Difference between scalar and vector approach.

AMTD
8, 4917–4971, 2015

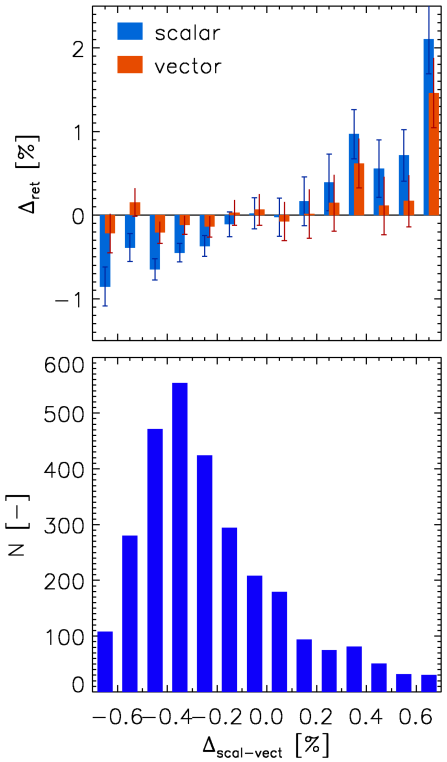

Figure 17. Effect of the radiative transfer solver on Δ_{ret}. (Upper panel) Total ozone column retrieval error as a function of difference between scalar and vector approach, (lower panel) number of validation points. The analysis is based on measurements at Lerwick, de Bilt, Churchill B-MKIV.032, Goose Bay, Hong Kong Obs., Izaña.

AMTD
8, 4917–4971, 2015

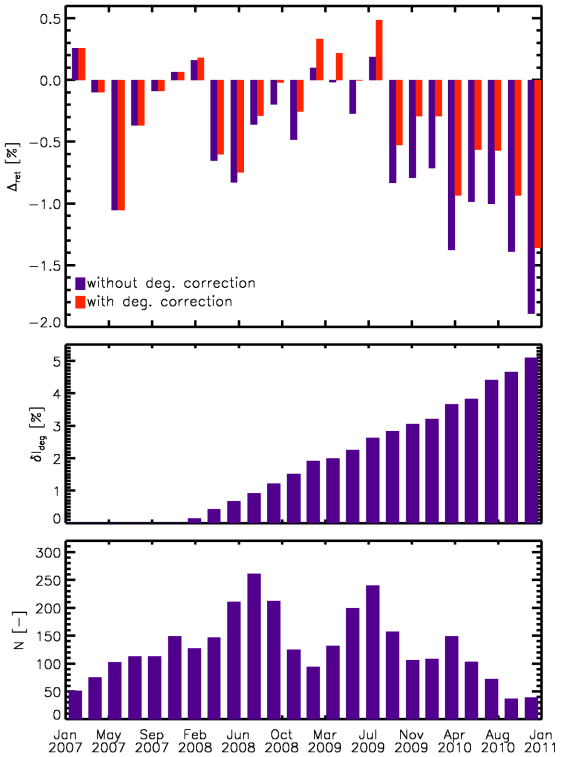

Figure 18. (Top panel) Time series of the total ozone column retrieval error (Δ_{ret}) with (red) and without (blue) degradation correction. (Middle panel) Degradation for the corresponding bin referenced to 2007. (Bottom panel) Data abundance for each bin. The data are acquired from collocations with Ankara, Churchill (Brewer MKII.026), De Bilt, Edmonton (Brewer MKII.055), Hohenpeissenberg, Hong Kong Observatory, Izaña, Naha, and Paramaribo.

AMTD
8, 4917–4971, 2015

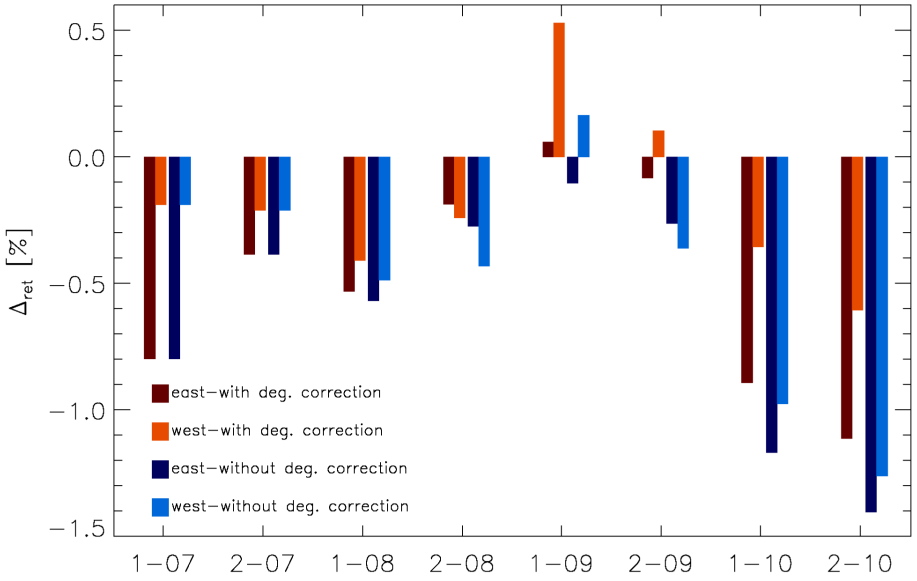

Figure 19. Influence of the scan angle dependent degradation on the total ozone column retrieval error (Δ_{ret}). Data are binned into six month intervals as well as east and west pixel bins, separated between pixel numbers 12 and 13 (Fig. 2). The lighter colours indicate the western pixels and the darker colours the eastern pixels. Furthermore, blue colours represent the data not corrected for degradation and the orange-brown colours the degradation corrected data. The underlying dataset is the same as in Fig. 18.

AMTD
8, 4917–4971, 2015